Luminescence of excitons

7

In an ideal pure semiconductor, the primary electronic excitation is a free electron–hole pair, the energy required for its creation (supplied, for example, by an incident photon) being equal—at the very minimum—to the bandgap value E_g. In a simplified way, an exciton may be visualized as a couple consisting of an electron and the associated hole, attracted to each other via Coulomb forces. Therefore, such a bound electron–hole pair no longer represents two independent quasi-particles and its internal energy is lower than E_g. The exciton is thus a quasi-particle representing the lowest electronic excitation in a semiconductor. There exist three basic types of excitons:

1. *Frenkel exciton* or a small-radius exciton. The spatial extension of the excitation is approximately restricted to a single unit cell. These excitons are to a large extent localized at a specific atom or molecule, and their movement through the crystal is limited to a hopping mechanism. They occur in molecular crystals.
2. *A charge transfer exciton* occurs primarily in ionic crystals. One can imagine its creation as follows: An electron is transferred from a lattice anion to a nearest neighbour cation, thereby creating there a maximum of the electron charge density. The radius of the charge transfer exciton can therefore be somewhat larger than that of the Frenkel exciton.
3. *Wannier exciton* or a large-radius exciton. The electron and hole are separated over many lattice constants, the exciton wavefunction is strongly delocalized and the exciton can move freely inside the crystal. Such a quasi-particle is also called a *free exciton*. The free exciton transfers the excitation energy, however, not the electric charge, because—as a whole—it is electrically neutral. Wannier excitons occur mainly in semiconductors.

The annihilation of an exciton is accompanied by a characteristic luminescence due to radiative recombination of the electron with the hole. In this chapter, we shall explain in detail the concept of the Wannier exciton and expound how it manifests itself in luminescence. Afterwards, we shall discuss the characteristic features of luminescence of the so-called bound excitons (i.e. excitons localized at impurity atoms or self-trapped owing to the strong exciton–phonon interaction).

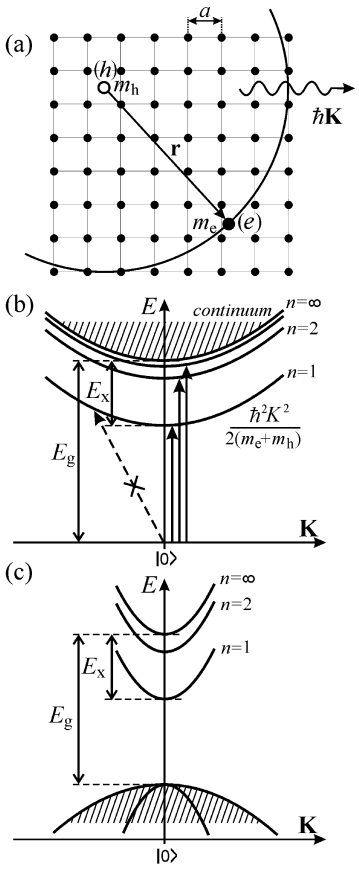

Fig. 7.1
(a) Schematic of the Wannier exciton in a two-dimensional crystal lattice with lattice constant a. Here $\hbar\mathbf{K}$ stands for the quasi-momentum belonging to the translational movement of the exciton centre of mass, and the effective masses of the electron (e) and hole (h) are denoted m_e and m_h, respectively. (b) The exciton dispersion relations $E = E(\mathbf{K})$. Optical absorption transitions are also marked; 'non-vertical' transitions are not allowed. (c) An incorrect plot of the exciton levels within the energy band scheme of a semiconductor (see text).

7.1 Concept of the Wannier exciton

The Wannier exciton can be conceived, in a first approximation, as a weakly bound electron–hole pair at which an electron and a hole circulate around each other; the attractive force results from the Coulomb potential

$$U(r) = -\frac{e^2}{4\pi\varepsilon_0\varepsilon\, r}, \tag{7.1}$$

where r is the electron–hole distance and ε stands for the dielectric constant of the substance. A striking resemblance with the hydrogen atom is already evident at first sight; the role of the proton is played here by the hole. If we regard the electron and hole as point charges characterized by their charge and effective masses (the so-called effective mass approximation), we can apply a modified Bohr model of the hydrogen atom. We shall see that this illustrative approximation can explain the majority of the principal features observed in the optical spectra of Wannier excitons in semiconductors.

Let us rotate the electron around the hole (which is always heavier, see Fig. 7.1(a)), thus circulating an orbit with radius r given by eqn (7.1). With regard to the Bohr radius of the hydrogen atom $a_B \approx 5 \times 10^{-2}$ nm, however, we encounter here two factors which impose the necessity of rescaling this characteristic length. Firstly, now we have a substantially different ratio of the (effective) masses. Unlike the pair of a light electron and a very heavy proton, the exciton is composed of two light quasi-particles with comparable masses m_e, m_h which entails a lower stability of the exciton in comparison with the hydrogen atom, and thus to a larger radius of the electron orbit. Secondly, the attractive electrostatic force between the electron and hole in a semiconductor is shielded by the dielectric constant ε,[1] which reduces further the attractive force and results in an increase in the orbital radius. It turns out that we may write

$$r_n = \frac{\varepsilon}{(m_r/m_0)} a_{Bn} = \frac{\varepsilon}{(m_r/m_0)} n^2 a_B, \tag{7.2}$$

where $n = 1, 2, 3, \ldots$ is the principal quantum orbit number, $m_r = (m_e m_h)/(m_e + m_h)$ is the reduced mass of the exciton and m_0 stands for the free electron mass. The commonly understood Bohr radius of the hydrogen atom a_B corresponds to the ground state, i.e. to the quantum number $n = 1 (a_B \equiv a_{B1})$. Considering typical values $\varepsilon \approx 10$ and $(m_r/m_0) \approx 0.1$ for a semiconductor, an order-of-magnitude estimate of the Wannier exciton ground state radius thus yields $a_X \equiv r_1 \approx 100 a_B \approx 5$ nm.

Let us rescale in a similar way the binding (or ionization) energy of the hydrogen atom. It is well known that this energy, commonly known as one Rydberg, amounts to 13.6 eV and refers to the ground state of the hydrogen atom. Let us denote $Ry(\mathrm{H}) = 13.6$ eV. As noted above, the low value of the

[1] A completely independent issue is whether the static ε_s or high-frequency ε_∞ dielectric constant is to be applied. This question has not yet been clarified up to now. It depends on whether the volume occupied by the exciton is large enough in order to be regarded as a homogeneous dielectric. Most frequently, the so-called Haken correction which interpolates between ε_s and ε_∞ is used.

Table 7.1 The binding energy and Bohr radius of free excitons in selected semiconductors. The width (E_g) and type (d–direct, i–indirect) of the bandgap are indicated.

Semiconductor	Binding energy E_X (meV)		Radius a_X (nm)	E_g (eV) i/d
	experimental	calculated		
CuCl	190		0.7	3.395 d
CuBr	108		1.25	3.077 d
Cu_2O	150		0.5	2.17 d
ZnS	36			3.78 d
AgBr	~ 22		~ 3	2.71 i
GaN	28	23	3.1	3.49 d
ZnO	61	~ 58		3.44 d
TlCl	23^{i}, 11^{d}			3.22i/3.42d
AgCl	23			3.27 i
TlBr	19^{i}, 9^{d}		2.6^{i} 4.1^{d}	2.66i/3.02d
GaP	18	21		2.35 i
ZnSe	19	20	4.5	2.8 d
CdS	30	28	2.7	2.58 d
ZnTe	13	13	5.5	2.39 d
CdSe	15	15	5.4	1.83 d
CdTe	10.5	12	6.7	1.60 d
GaAs	4.2	4.9	13	1.52 d
InP	5.1	4.8	12	1.42 d
Si	14.7	14.7	4.9	1.17 i
Ge	4.15	4.17	11.4	0.74 i
GaSb	2.8	2	23	0.81 d
InSb		0.4	100	0.23 d
SiC	28			2.42i

reduced mass (m_r/m_0) along with the high dielectric constant reduces the stability of the exciton. The exciton energy levels are therefore expected to lie markedly closer to the ionization continuum in comparison with the hydrogen atom:

$$E_{X(n)} = \frac{(m_r/m_0)}{\varepsilon^2}\frac{1}{n^2}Ry(\mathrm{H}) = \frac{E_X}{n^2}. \tag{7.3}$$

The binding energy, denoted E_X in eqn (7.3), corresponds to the exciton ground state $n = 1$, therefore

$$E_X \equiv E_{X(1)} = \frac{(m_r/m_0)}{\varepsilon^2}Ry(\mathrm{H}). \tag{7.4}$$

A typical value of E_X thus amounts to $E_X \approx (0.1/10^2) \times 13.6\,\mathrm{eV} \approx 13\,\mathrm{meV}$. The Wannier exciton *binding energy* is therefore of the order of tens of meV. The exciton is stable only if the attractive potential (7.1) is strong enough to prevent the exciton from breaking up owing to collisions with phonons. The binding energy E_X must thus be higher than $\sim k_B T$. Because the value $k_B T = 10\,\mathrm{meV}$ is associated with $T \approx 110\,\mathrm{K}$, one comes to the important conclusion that excitons in semiconductors occur only at low temperatures. Table 7.1 summarizes the basic exciton parameters in selected semiconductors.

To understand the next properties of the Wannier exciton, we have to go a step beyond the effective-mass approximation. From the point of view of wave–particle duality, it is possible to describe an exciton by its wavefunction and to tackle the problem of finding its stationary energy states using the standard methods of solid-state quantum theory [1, 2]; they lead to expressions (7.2) and (7.3). The exciton wavefunction, which is constructed as a linear combination of atomic functions of the crystal, has the same translational symmetry as the crystal lattice. The larger or smaller extent of the exciton's spatial localization (corresponding to its Bohr radius a_X) is described in quantum mechanics by the so-called envelope wavefunction.

Free excitons may thus move throughout the lattice. The following quantities are associated with such a translational movement: the exciton wavevector $\mathbf{K}$, quasi-momentum $\hbar\mathbf{K}$ and kinetic energy $E_{kin} = \hbar^2 K^2/2(m_e + m_h)$. Considering eqn (7.3), the total exciton energy can then be written in the form

$$E_{(n)}(\mathbf{K}) = E_g - E_{X(n)} + E_{kin} = E_g - \frac{(m_r/m_0)}{\varepsilon^2}\frac{Ry(H)}{n^2} + \frac{\hbar^2 K^2}{2(m_e + m_h)}. \tag{7.5}$$

For the ground state, $n = 1$, energy we thereby get

$$E_{(1)}(\mathbf{K}) = E_g - E_X + \frac{\hbar^2 K^2}{2(m_e + m_h)} = E_g - E_X + \frac{\hbar^2 K^2}{2m_{exc}}, \tag{7.6}$$

where $m_{exc} = m_e + m_h$ is the total (or effective) exciton mass. Here, it is necessary to stress that, in addition to low temperatures, also sufficient *purity of the crystal* is essential for free excitons to exist. That is, the impurity atoms represent very efficient traps for the free excitons propagating through the crystal, which then get localized at the impurities (losing their kinetic energy) and *bound excitons* are created.

Equations (7.5) or (7.6) are nothing but the dispersion relations of a free exciton. They are depicted in Fig. 7.1(b). This figure looks very similar to a commonly used representation of the semiconductor band structure, just some extra discrete exciton levels within the bandgap appear. However, there is a substantial difference—the common energy band scheme of a semiconductor follows from the so-called one-electron approximation in which one chosen test electron moves in the effective potential of electric forces exerted by all of the other electrons and periodically arranged atomic cores. The exciton concept goes beyond this one-electron approximation because it takes into consideration the extra influence of a positive hole. Therefore, the scheme in Fig. 7.1(b) no longer belongs to the one-electron approximation and the $\mathbf{K} = |0\rangle$ point cannot be identified with the top of the valence band; it represents the ground state of the whole ideal pure crystal where all the spin and orbital electron momenta are compensated.

What may be somewhat misleading is that these exciton levels can in fact be formally drawn also into the one-electron scheme, which is depicted in Fig. 7.1(c). Even if one can meet similar pictures in renowned textbooks, this approach is not fully accurate and might lead to an incorrect interpretation of such schemes, as we shall see in Chapter 8.

7.1.1 Absorption spectrum of the Wannier exciton

Before we set about the exposition of exciton luminescence (i.e. light emission) properties accompanying the annihilation of the exciton, we describe how the creation of an exciton due to the absorption of an appropriate incident photon manifests itself in the optical absorption spectra of semiconductors.

Let us first consider a direct-bandgap semiconductor. It is well known that the onset of the absorption edge here is described (in the so-called dipole approximation and without considering the exciton effects) by the square-root law [2–4]

$$\alpha(h\nu) \approx (h\nu - E_g)^{1/2}, \quad h\nu \geq E_g. \tag{7.7}$$

The photons possessing energy $h\nu$ smaller than the bandgap width E_g therefore should not be absorbed at all. In fact, however, very distinctive absorption lines at certain discrete energies $h\nu < E_g$ are observed experimentally at low temperatures. Their origin is depicted by the upward arrows in Fig. 7.1(b), namely, they arise from transitions from the $|0\rangle$ state to the $n = 1$ state (creation of the exciton in its ground state) and to the higher exciton levels $n = 2, 3, \ldots$ This is thus the characteristic and famous hydrogen-like series in the absorption spectra, comprising lines at energies

$$h\nu = E_g - \frac{E_X}{n^2}, \quad n = 1, 2, 3, \ldots \infty; \tag{7.8}$$

the band-to-band absorption to the states labelled in Fig. 7.1(b) as 'continuum' begins by transitions to $n = \infty$.

It becomes clear by comparing (7.5) and (7.8) that the excitons created by this kind of light absorption have zero kinetic energy. In other words, the excitons at $\mathbf{K} = |0\rangle$ are created by vertical transitions. The question arises as to whether also 'non-vertical' transitions as indicated in Fig. 7.1.(b) can occur. The answer is no; they cannot, because the relation $\lambda \gg a$ holds between the optical wavelength $\lambda = c/\nu$ and the lattice constant a. The magnitude of the photon wavevector $2\pi/\lambda$ is therefore negligible compared with the characteristic dimension of the Brillouin zone $2\pi/a$ and, consequently, the quasi-momentum of the absorbed photon, is not sufficient to ensure the necessary change of $\mathbf{K}$ required for the non-vertical transition. Such a transition would thus have to incorporate a third quasi-particle—phonon—and the absorption act would then be classified as a higher-order process, the probability of which is many orders of magnitude lower.

A textbook example of the direct-bandgap absorption spectrum in the exciton region is given in Fig. 7.2 (pure GaAs at $T = 1.2\,\mathrm{K}$) [5]. Two additional important facts follow from this figure. Firstly, the intensity of the absorption lines drops with increasing n (proportionally to $\sim 1/n^3$), and, secondly, the optical absorption for $h\nu \geq E_g$ becomes enhanced under the influence of excitons (the absorption edge shape without considering the exciton effects, as given by eqn (7.7), is depicted by the dashed line).

In a direct-bandgap semiconductor in which the dipole transitions in the vicinity of the absorption edge are not allowed owing to the symmetry of the wavefunction in the band extrema (Cu_2O), the absorption spectrum has

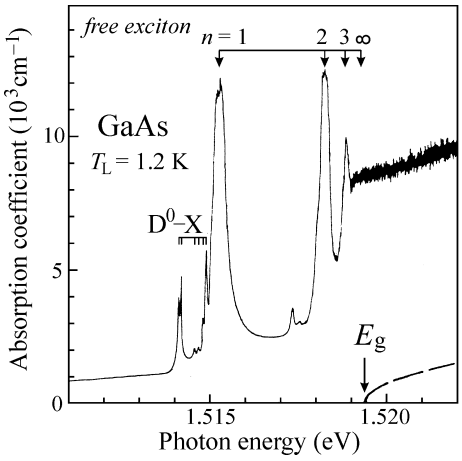

Fig. 7.2
Optical absorption spectrum of a very pure GaAs sample at $T = 1.2$ K in the vicinity of the absorption edge. Marked absorption lines, leading to the creation of the free exciton in the state $n = 1, 2$ and 3, dominate the spectrum. Absorption into higher exciton states merges gently into the absorption continuum; the value of the forbidden gap $E_g = 1.5194$ eV is determined by extrapolating the series to $n = \infty$. The dashed line at the bottom right represents the absorption edge shape $(h\nu–E_g)^{1/2}$ expected in the absence of the electron–hole interaction. D^0–X stands for the absorption on residual impurities. After Weisbuch and Benisty [5].

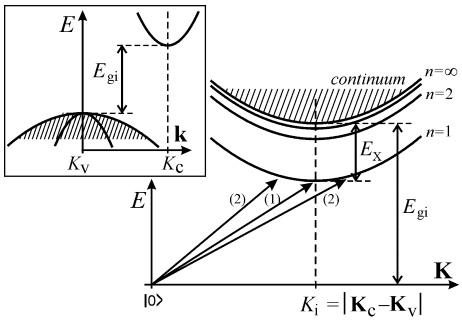

Fig. 7.3
Exciton dispersion relations in a semiconductor with indirect bandgap of width E_{gi}. The arrows indicate optical absorption transitions from the $|0\rangle$ point. The inset shows the relevant electronic band structure in the one-electron approximation.

a somewhat different character (the line intensity decreases proportionally to $(n^2–1)/n^5$ and the $n = 1$ line is missing). However, the marked absorption lines still dominate the spectrum.

In indirect-bandgap semiconductors, however, a substantially different spectral dependence around the onset of the intrinsic absorption edge occurs. The situation is schematically depicted in Fig. 7.3. The $\mathbf{K} = |0\rangle$ point again represents the crystal ground state, however, the exciton dispersion curves have a minimum at $\boldsymbol{K}_i = |\mathbf{K}_c–\mathbf{K}_v|$, where $\mathbf{K}_c(\mathbf{K}_v)$ stands for the wavevector of the conduction (valence) band extremum, respectively; see the inset in Fig 7.3. A stable exciton can be created only when the group velocities of the electron and hole are the same; only in this case can the electron and hole move together as a bound pair. Since the electron or hole group velocity in the band is equal to

$$\mathbf{V}_g = \frac{1}{\hbar}\frac{\partial E}{\partial \mathbf{k}}, \tag{7.9}$$

the claim for equality of the group velocities (zero gradient) will undoubtedly be fulfilled in the valence $\mathbf{K}_v$ and conduction $\mathbf{K}_c$ band extrema, therefore the

exciton created with a minimum energy will be characterized by the wavevector $K_i = |\mathbf{K}_c - \mathbf{K}_v|$.[2]

The onset of optical absorption should thus turn up at the photon energy $h\nu = E_{gi} - E_X$ (transition (1) in Fig. 7.3). However, because now a phonon $\hbar\omega$ with a wavevector $|\mathbf{K}_c - \mathbf{K}_v|$ must obviously participate in the absorption process in order to meet the quasi-momentum conservation law, the threshold value of the photon energy will shift to $h\nu = E_{gi} - E_X + \hbar\omega$ (we consider only low temperatures and hence the *phonon emission* into the lattice reservoir). Besides, the values of the absorption coefficient will be much lower compared with direct-gap semiconductors and—what is most important—there is no reason to observe any absorption lines, because the transitions (2) in Fig. 7.3 will have the same probability as the transition (1), both types of process being of the same order. Then the density of states in the exciton bands, proportional to $[E - (E_{gi} - E_{X(n)})]^{1/2}$, enters the play and the absorption coefficient will increase with increasing $h\nu$ starting from the threshold values $E_{gi} - E_{X(n)} + \hbar\omega$. Such a spectral course of the absorption coefficient is schematically depicted in Fig. 7.4(a). Instead of discrete lines, it contains characteristic 'shoulders' at the energies $E_{gi} - E_{X(n)} + \hbar\omega$. An example of a simple experimental exciton absorption spectrum of an indirect-bandgap semiconductor (AgBr) is shown Fig. 7.4(b) [6]. In reality, the experimental spectrum often shows a somewhat richer structure than that displayed in Fig. 7.4(b)—for instance in Si and Ge—as a consequence of the higher number of various types of participating phonons. Then, however, the analysis of such a spectrum is not an easy task.

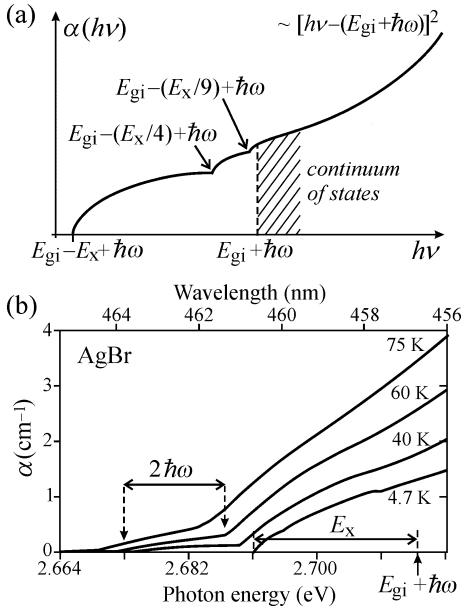

Fig. 7.4
(a) Schematic drawing of the low-temperature exciton absorption spectrum in an indirect-bandgap semiconductor. (b) Measured temperature dependence of the exciton absorption spectrum in AgBr. The drawing (a) corresponds to the curve recorded at $T = 4.7$ K. The value of $(E_{gi} + \hbar\omega) \approx 2.714$ eV (determined with the help of the binding energy value $E_X \approx 22$ meV established from other measurements) is indicated. As the temperature rises, a shift of E_{gi} towards lower energies occurs on the one hand and, on the other, absorption processes with phonon annihilation begin to operate, resulting in the occurrence of another shoulder red-shifted by $2\hbar\omega$. Thence it is possible to determine the energy of the quasi-momentum conserving phonon: $\hbar\omega \cong 8$ meV (TO(L)). After Joesten and Brown [6].

[2] In direct-bandgap semiconductor $\mathbf{K}_c = \mathbf{K}_v = 0$ holds and thus the exciton is created at $\mathbf{K} = |0\rangle$, in accordance with the previous discussion.

It is worth noting that the transitions of type (2) result in the appearance of excitons with non-zero kinetic energy, unlike direct-bandgap semiconductor where the resonant condition (7.8) leads to the creation of excitons with zero kinetic energy. However, it is important to realize that in both the types of semiconductors, excitons with non-zero kinetic energy can be created easily by optical absorption in the 'non-resonant' way. By means of photons $h\nu > E_g$ one creates free electron–hole pairs which are very quickly, in the order of picoseconds, bound to excitons. These thermalize rapidly, getting rid of the excess energy through the emission of phonons into the lattice. Such an exciton gas can be described statistically by its kinetic energy distribution with a certain effective temperature, as was explained in Section 5.3.

7.1.2 Direct bandgap: resonant luminescence of free exciton–polaritons

Looking at Fig. 7.1(b), an idea about exciton luminescence may cross our mind, namely, that luminescence transitions accompanying exciton annihilation can be depicted simply by turning upside down the arrows pointing up from $|0\rangle$ to $n = 1, 2, \ldots$. In the *emission spectrum* thereby a series of lines fully analogous to the lines shown in the *absorption spectrum* in Fig. 7.2 will appear (at least, it works like this in the case of a hydrogen atom). Unfortunately, this is not quite true. Here, the difference between a gas of non-interacting hydrogen atoms and the collective properties of the solid state will reveal itself, as well as the influence of residual impurities which are present even in nominally pure undoped semiconductor materials. The situation around the luminescence of free excitons thus becomes rather complicated.

The luminescence photon, created during exciton annihilation due to the radiative recombination of the electron with a hole, will be resonantly reabsorbed while travelling through the lattice (the absorption coefficient for exciton absorption lines is very high – see Fig. 7.2) and transformed back into an exciton; this exciton, when its lifetime is out, annihilates emitting a photon which is again reabsorbed, and so on. Such an oversimplified 'mechanistic' view is evidently untenable; however, it points to the fact that the concepts of the exciton and photon inside a solid can hardly be separated from each other. We speak of a mixed electronic-polarization and optical wave propagating through the crystal, for which the term *polariton* (not to be confused with polaron!) or more strictly *exciton–polariton* is used.[3]

A more solid idea about polaritons and their luminescence can be obtained from the graphical representation of their dispersion curves $E(\mathbf{K})$. The dispersion curves of the exciton $E(\mathbf{K}) = E_g - E_X + \hbar^2 K^2/2m_{exc}$ and of a bare photon $E(K) = h\nu = \hbar c K/\sqrt{\varepsilon_\infty}$ (i.e. the straight line with slope $\hbar c/\sqrt{\varepsilon_\infty}$) without considering the above mentioned interaction are schematically depicted in Fig. 7.5(a). Both curves must necessarily cross each other. However, it is known that in a degenerate quantum system, the degeneracy is

[3] Analogously, one can encounter a *phonon–polariton* in the infrared part of the spectrum in polar crystals.

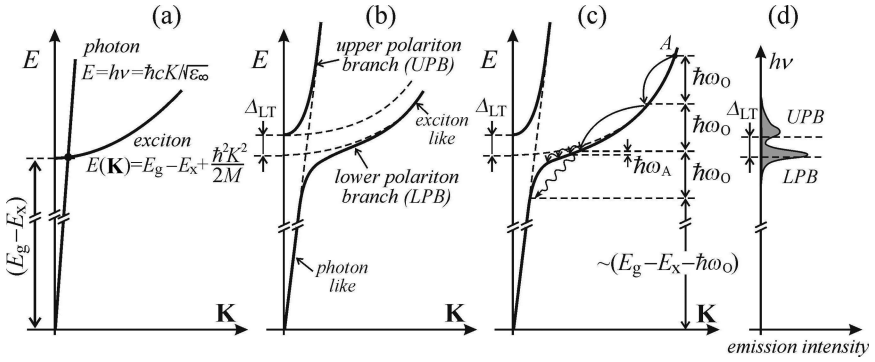

Fig. 7.5
(a) Dispersion curve of a 'bare' exciton and 'bare' photon (straight line with slope of $\hbar c(\sqrt{\varepsilon_\infty})^{-1}$), i.e. without considering their mutual interaction. (b) Schematic of the exciton–polariton dispersion curves. Δ_{LT} stands for the longitudinal-transverse exciton splitting. (c) Thermalization of LPB polaritons owing to the cascade emission of optical ($\hbar\omega_{\mathrm{O}}$) and acoustic ($\hbar\omega_{\mathrm{A}}$) phonons. (d) Schematic of the luminescence spectrum of polaritons.

lifted owing to the interaction. Here, it means simply that a splitting of the curves in the vicinity of this point of intersection will appear, as suggested in Fig. 7.5(b). Moreover, the so-called longitudinal-transverse splitting Δ_{LT} of the exciton gains importance in polar cubic semiconductors, in analogy with the energy difference between LO- and TO-phonons (Section 4.2). The resulting polariton dispersion curves are drawn by solid lines in Fig. 7.5(b). One can indeed recognize around the intersection point a region having the character of mixed exciton-photon states, while far from this point the curves have a character very similar to a bare photon (the so-called 'photon-like' straight lines with a slope close to the value of $\hbar$ multiplied by the light velocity) or to a bare exciton with the characteric parabolic dependence $E \sim K^2$. The entire dispersion curve is then composed of two branches, namely, the upper polariton branch (UPB) and the lower polariton branch (LPB).

The existence of these two branches and, in particular, of the strong LPB curvature around the point where the 'photon-like' straight line turns into the 'exciton-like' parabola $\sim \hbar^2 K^2/2m_{\mathrm{exc}}$, is essential for understanding the shape of the polariton emission spectra. This region in the $(E, \mathbf{K})$ plane is often termed a *bottleneck*.

Let us consider a common situation during which the polaritons are created (non-resonantly) via absorption of photons with energy high above the bandgap as, for example, at A point in Fig. 7.5(c). Thermalization of these polaritons runs initially—far away from the 'bottleneck'—very efficiently via emission of the optical phonons possessing a high energy $\hbar\omega_0$ at $\mathbf{K} \approx 0$; close to the bottleneck, however, the scattering to lower energy states can be mediated only via emission of the acoustic phonons with very low energy $\hbar\omega_{\mathrm{A}}$. Naturally, the thermalization process is slowing down significantly and a considerable accumulation of the polariton population on the LPB in the vicinity of the bottleneck will occur. A similar accumulation is likely to happen also near the bottom of the UPB. After a lapse of their lifetime of the order of

10^{-9} s, these accumulated polaritons 'recombine' to give rise to a no-phonon[4] exciton–polariton luminescence that, localized spectrally in the close vicinity of $h\nu \approx (E_g – E_X)$, emerges from the crystal. The emission spectrum thus consists, according to what has just been said, of two lines separated by $\sim \Delta_{LT}$. This is schematically depicted in Fig. 7.5(d). The line originating from the LPB branch is usually more intense, as may be inferred from thermodynamic considerations. It is necessary to emphasize, however, that no simple analytic formula describing the corresponding spectral lineshape like, e.g., eqns (5.9) or (5.13) exists, in spite of numerous attempts to deduce such a lineshape formula theoretically.

It may be interesting to mention that this spectral shape actually complies with the original simple concept of the excitonic luminescence reabsorption—the central part of a narrow emission line is (seemingly?) reabsorbed and only both of the wings survive (see also Appendix H).

Figure 7.6 shows an example of the experimental emission spectrum of the exciton–polariton in GaAs at $T = 4.2$ K [7]. The thick arrow marks the position of the $n = 1$ absorption line (i.e. $h\nu = E_g – E_X$), taken from Fig. 7.2. A qualitative agreement with Fig. 7.5(d) is evident.

The above discussed model of the exciton–polariton luminescence was refined by Koteles *et al.* [8] who noticed that the occurrence of the 'UPB/LPB doublet' was affected to a large extent by the concentration of residual impurities, in particular donors. The authors assume that all the excitons, after having thermalized, accumulate exclusively on the LPB branch and, accordingly, their luminescence spectrum should consist of a single line only. However, if donors are present at a relatively high concentration ($\geq 10^{15}$ cm^{-3}), the exciton–polaritons are scattered on their way from the bulk by elastic collisions just with these donors (not by acceptors because their Bohr radius—which means, in this case, their effective scattering cross-section—is

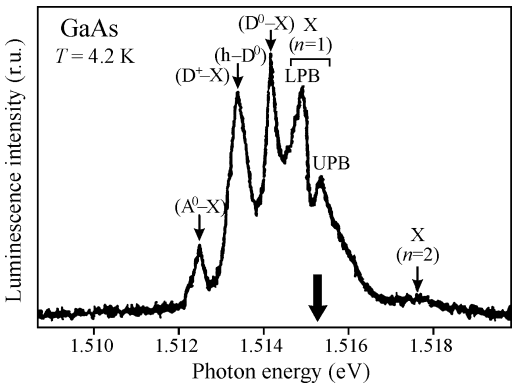

Fig. 7.6
Luminescence spectrum of free exciton–polariton X in very pure GaAs at $T = 4.2$ K (impurity concentration of the order of 10^{13} cm^{-3}). Lines due to the upper (UPB) and lower (LPB) polariton branch in the $n = 1$ state are clearly evident. The thick arrow marks the position of the *absorption* line $n = 1$. The line labelled (h–D^0) is caused by the recombination of a hole with a neutral donor (Section 5.3); lines (D^0–X) and (A^0–X) are due to recombination of bound excitons (Section 7.2). On the right, a weak indication of a line arising from recombination of the $n = 2$ state of the exciton–polariton can also be seen. After Razeghi *et al.* [7].

[4] That is, phonons do not participate in the actual emission process. However, it is possible to conceive of a process (depicted by the lower wavy line in Fig. 7.5(c)), during which emission of another phonon $\hbar\omega_0$ occurs and, at the same time, the polariton moves to the photon part of the dispersion curve. This means that the radiative decay of the exciton–polariton is accompanied by emission of an optical phonon. We shall treat this mechanism shortly.

substantially lower!). This scattering leads, according to detailed calculations, to a 'hole burning' in the luminescence line profile and to the emergence of the doublet. In sufficiently pure samples polariton scattering does not occur. Very convincing support for this theory is given in Fig. 7.7, which depicts three photoluminescence spectra of nominally undoped epitaxial GaAs layers with different residual donor concentrations. Incontestably, the free exciton (X) line splitting fades away with increasing sample purity. The effect seems to be confirmed by more and more frequent observation of a simple and intense luminescence line at the $n = 1$ position of the free exciton also in other materials, e.g. InP (Fig. 7.8) [9]. This tendency is likely to be closely related to the incessant improvement of a wide range of preparation techniques of ultrahigh-purity semiconductors, such as molecular beam epitaxy (MBE) or metal organic vapour phase epitaxy (MOVPE), etc. Figures 7.6–7.8 can serve as examples of a photoluminescence assessment of the semiconductor purity that shows a considerable application impact, and is *de facto* a unique and irreplaceable method used even in the microelectronics industry. Application of this photoluminescence impurity analysis in the case of silicon, where it even gives quantitative information, will be discussed in detail in Subsection 7.2.2.

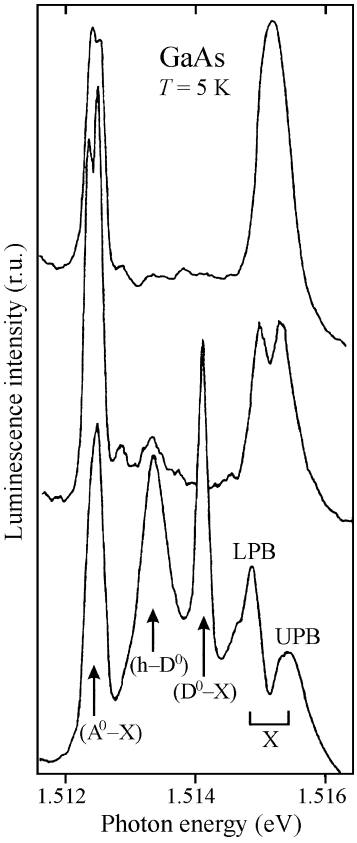

Fig. 7.7
Emission spectra of three undoped epitaxial layers of GaAs with different residual donor concentrations. The bottom spectrum belongs to the sample with the highest concentration of donors, and this concentration decreases towards the middle and upper spectra. At the same time it can be seen that the free exciton-polariton line (X) is losing its splitting into the UPB and LPB. Bath temperature is 5 K. Labelling of the remaining lines is the same as in Fig. 7.6. After Koteles *et al.* [8].

7.1.3 Direct bandgap: luminescence of free excitons with emission of optical phonons

The previous subsection might have evoked an impression that the entire spectral manifestation of free exciton luminescence in a direct-bandgap semiconductor is characterized by a kind of not-very-exactly defined lineshape which often almost disappears in the background of plenty of other emission lines. Nevertheless, there exists another intrinsic free exciton recombination channel in direct-bandgap semiconductors, significant especially in II-VI type semiconductors, namely, luminescence with simultaneous emission of LO-phonons (possibly TO-phonons, as well). Specific for this channel is a pronounced emission line (or even a series of lines) with a well-defined spectral shape.

This process, as we have already mentioned, is depicted by the lower wavy line in Fig. 7.5(c). From here we can at once estimate the spectral position of the relevant line as

$$h\nu_{\mathrm{X}-m\,\mathrm{LO}} \approx (E_{\mathrm{g}} - E_{\mathrm{X}}) - m\,\hbar\omega_0, \quad m = 1, 2, 3, \ldots \tag{7.10}$$

This relation formulates nothing but the law of energy conservation, expressing that the lines are shifted, with respect to the exciton–polariton resonant line (or 'doublet'), towards lower energies by a multiple of the phonon energy $\hbar\omega_0$. (Figure 7.5(c) shows this recombination for $m = 1$ only.) In the literature these lines are sometimes marked as A–LO, A–2LO, ..., or X–LO, X–2LO, etc. Their intensity is relatively high but, at the same time, the reason for this is not obvious at first sight—after all, one deals with a process incorporating the participation of a third quasi-particle and thus its probability to occur should

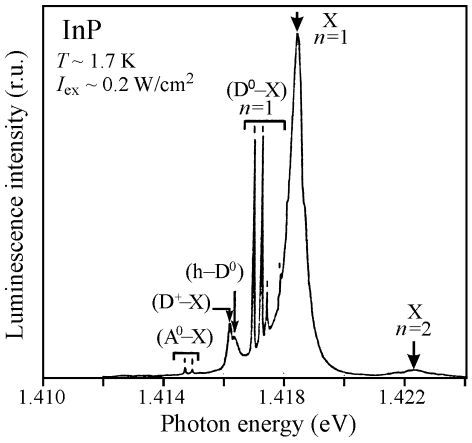

Fig. 7.8
Emission spectrum of a pure epitaxial layer of InP (residual impurity concentration below 10^{14} cm^{-3}). The spectrum is dominated by an unsplit line of the exciton–polariton ground state ($X_{n=1}$); a weak trace of the first exciton–polariton excited state ($X_{n=2}$) is also present. Other lines on the low-energy side of the spectrum are attributed to recombination of an exciton bound to a neutral donor in the ground state $(D^0–X)_{n=1}$, an exciton bound to an ionized donor (D^+–X), exciton bound to a neutral acceptor (A^0–X) and to recombination of a hole with a neutral donor (h–D^0). Notice that the bound exciton linewidth is much narrower in comparison with the linewidth of the free exciton–polariton; the latter reflects the kinetic energy distribution in the free exciton gas. After Bose *et al.* [9].

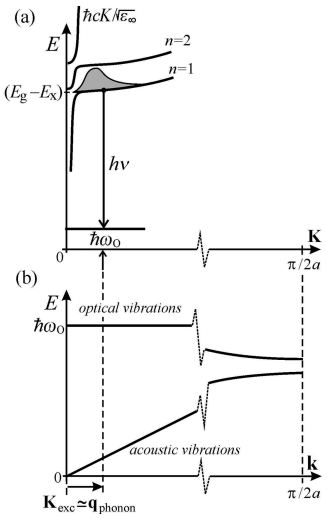

Fig. 7.9
(a) Radiative recombination of a free exciton accompanied by emission of one optical phonon. The photon energy is $h\nu \approx (E_g - E_X) - \hbar\omega_0$, the quasi-momentum conservation law $\mathbf{K}_{exc} \cong \mathbf{q}_{photon}$ is satisfied. The shaded area labels the Maxwell–Boltzmann distribution of the exciton kinetic energies. In the vicinity of $\mathbf{K} = 0$, a splitting of polariton states into UPB and LPB for both $n = 1$ and $n = 2$ is indicated. (b) Corresponding phonon dispersion curves.

be substantially lower than that of the resonant emission itself. The reasons for this are in fact two:

1. The emitted phonon delivers part of the energy of the decaying exciton–polariton into the lattice, thereby lowering the energy of the luminescence photon by multiples of $\hbar\omega_0$. The photon may thus escape to a large degree (but not completely) from the bottleneck region and circumvent number the resonant polariton complications (reabsorption and scattering). Therefore, a large number of photons finally reaches the sample surface and leaves the semiconductor.
2. The participation of phonons makes it possible for *all* the free excitons residing at the LPB (which have a certain distribution of their kinetic energy $\hbar^2 K_{exc}^2/2m_{exc}$ characterizing their propagation through the crystal) to take part in the radiative recombination process. This is because the participating phonons ensure the quasi-momentum conservation law $\mathbf{K}_{exc} \approx \mathbf{q}_{phonon}$ to be satisfied for the whole exciton population, while it is only exciton–polaritons with virtually zero kinetic energy, i.e. a zero wavevector $\mathbf{K}_{exc} = \mathbf{K}_{photon} \approx 0$, that can undergo resonant no-phonon radiative recombination. Such excitons, however, represent only a small fraction of the whole free exciton population, as shown in Fig. 7.9(a) (see also Problem 7/1). This is therefore the second reason why phonon participation in the emission process substantially increases the $(X - mLO)$ line intensity. (Sometimes one speaks of 'recoil' phonons released during the radiative annihilation of excitons.)

Now, one can anticipate intuitively that shapes of the emission lines with phonon participation will reflect the Maxwell–Boltzmann distribution of the free exciton kinetic energy and will thus be analogous to eqn (5.9). Basically this is the case; nevertheless, some small differences appear.

The lineshape should reflect in some way the probability of phonon(s) creation $W^{(m)}(m\mathbf{q}_{phonon})$; this is a new factor that we did not have to take into

account while deriving the relation (5.9); phonons did not participate there. We thus write formally

$$I_{\mathrm{sp}}^{(m)}(h\nu) \approx (h\nu - [(E_{\mathrm{g}} - E_{\mathrm{X}}) - m\hbar\omega_0])^{1/2} \times \exp\left[-\frac{h\nu - [(E_{\mathrm{g}} - E_{\mathrm{X}}) - m\hbar\omega_0]}{k_{\mathrm{B}}T}\right] W^{(m)}(m\mathbf{q}_{\mathrm{phonon}} \approx K_{\mathrm{exc}}), \tag{7.11}$$

considering simultaneously that the low-energy threshold of the line is given by eqn (7.10). Let us pay attention only to the (X–LO) and (X–2LO) lines, i.e. $m = 1, 2$. The quasi-momentum conservation law for one- and two-phonon assisted radiative annihilation of a free exciton is depicted in Fig. 7.10. During the one-phonon process (Fig. 7.10(a)), each exciton with a given $\mathbf{K}_{\mathrm{exc}}$ can create only phonons with essentially a discrete spectrum of magnitudes of their wavevectors $|\mathbf{q}_{\mathrm{phonon}}|$. The important question now reads: will the probability $W^{(1)}(\mathbf{q}_{\mathrm{phonon}})$ be the same for all excitons with different kinetic energy, i.e. with a different vector $\mathbf{K}_{\mathrm{exc}} \approx \mathbf{q}_{\mathrm{phonon}}$? The answer is no, because the moduli of all these vectors are small in comparison with the dimensions of the first Brillouin zone, and any of their relative variations $|\Delta\mathbf{q}|/|\mathbf{q}|$, however small they may be, is important. It can be expected that phonons whose *wavelengths* are comparable with the linear *dimension of the exciton* will be emitted most probably; therefore, the modulus of their wavevector will correspond to the modulus of the exciton wavevector. More accurate theoretical considerations lead to a scaling of the type $W^{(1)}(\mathbf{q}_{\mathrm{phonon}} \approx \mathbf{K}_{\mathrm{exc}}) \sim K_{\mathrm{exc}}^2$. In other words, $W^{(1)}$ is proportional to the exciton kinetic energy which

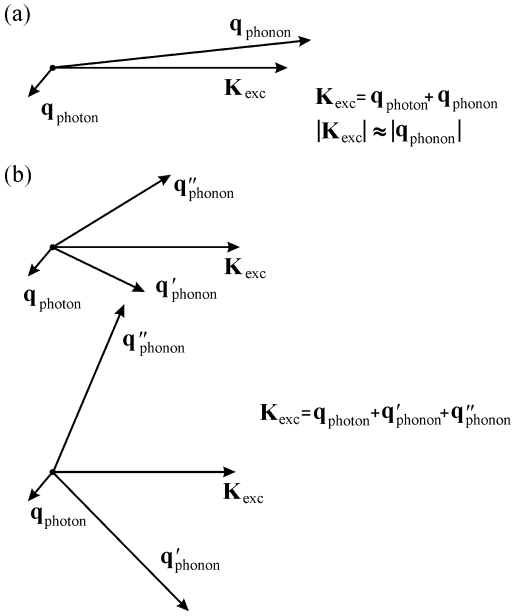

Fig. 7.10
Vector diagrams depicting the quasi-momentum conservation law during radiative annihilation of a free exciton: (a) with emission of one phonon, (b) with emission of two phonons.

is $(h\nu - [(E_g - E_X) - \hbar\omega_0])$. Therefore, for the (X–LO) process we obtain from (7.11)

$$I_{sp}^{(1)}(h\nu) \approx (h\nu - [(E_g - E_X) - \hbar\omega_0])^{3/2} \exp\left[-\frac{h\nu - [(E_g - E_X) - \hbar\omega_0]}{k_B T}\right]. \tag{7.12}$$

We emphasize once more that the scaling $W^{(1)} \sim |\mathbf{K}_{exc}|^2$ follows from the fact that the moduli of the exciton and phonon wavevectors are in this case comparable.

Two-phonon radiative recombination (X–2LO) satisfies the quasi-momentum conservation law in a slightly different way. The number of corresponding combinations of wavevectors $(\mathbf{q}'_{phonon}, \mathbf{q}''_{phonon})$ for each recombining exciton is high, and their moduli may be much larger than $|\mathbf{K}_{exc}|$, as can be seen in Fig. 7.10(b). Such phonons no longer 'feel' the spatial extent of the exciton, and one can expect $W^{(2)}(\mathbf{q}'_{phonon}, \mathbf{q}''_{phonon})$ to be no longer dependent upon the energy or upon the wavevector of the recombining exciton; thus $W^{(2)} = \text{const}$. It is this fact which causes the important difference between the one- and two-phonon process, and from (7.11) it follows immediately that the two-phonon lineshape ($m = 2$) will be Maxwell-like:

$$I_{sp}^{(2)}(h\nu) \approx (h\nu - [(E_g - E_X) - 2\hbar\omega_0])^{1/2} \exp\left[-\frac{h\nu - [(E_g - E_X) - 2\hbar\omega_0]}{k_B T}\right]. \tag{7.13}$$

These qualitative considerations were put forward for the first time by Gross *et al.* [10] and confirmed by quantum-mechanical calculations by Segall and Mahan [11]. Figure 7.11 reproduces (a) one of the first published emission spectra by Gross *et al.* in the spectral range of the $(X - m\,LO)$ lines in CdS [10], and (b) a comparison of the experiment with the theoretical lineshape (7.12) in CdSe [12].

The second important feature of the emission lines (X–LO), (X–2LO),..., contributing to their identification, is their intensity dependence. The free exciton recombination, as a typical intrinsic 'monomolecular' process, increases with the excitation linearly in a wide interval of excitation intensities (no saturation is observed).

We have not yet given a full account of why just the *optical phonons* have to participate in phonon-assisted free exciton luminescence. In fact acoustic phonons could not make the relevant effect possible because at low values of $|\mathbf{q}_{phonon}|$, their energy is close to zero (Fig. 7.9(b)) and would not be sufficient to release photons from the bottleneck region, or—if you like—to enable them to escape from the resonant reabsorption. The optical phonons have a constant non-zero energy $\hbar\omega_0$ in the vicinity of $|\mathbf{q}_{phonon}| = 0$ and do not introduce any additional factor which could complicate the emission lineshape (7.12) or (7.13). But then the 'legal' question arises: Is the participation of the 'welcome' optical phonons allowed also by selection rules imposed by the crystal symmetry?

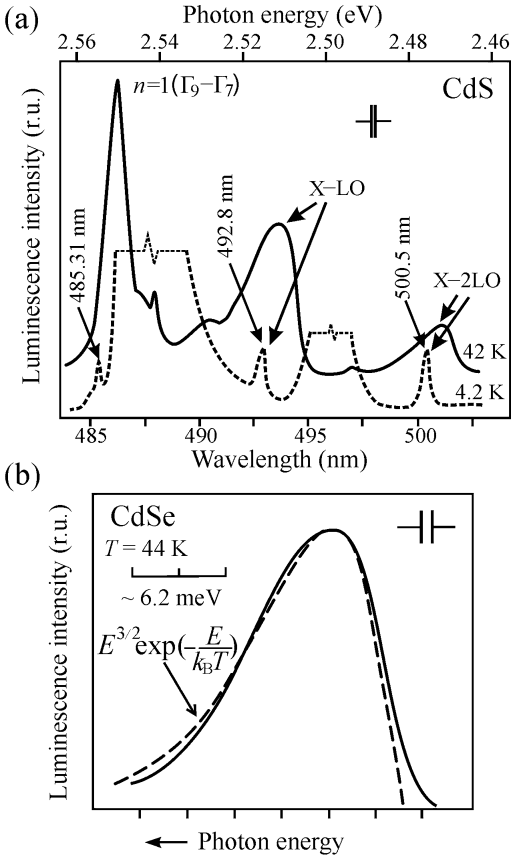

Fig. 7.11
(a) Emission spectrum of $n = 1$ free excitons (Γ_9–Γ_7) in CdS at $T = 4.2$ K (lower curve) and $T = 42$ K (upper curve). The lower curve from the left: a weak resonant line of the exciton–polariton (485.3 nm), a very intense and broad line (486–492 nm, intensity out of scale) due to an exciton bound to a residual impurity, a X–LO line at 492.8, once more an intense line of bound excitons (494–498) nm and finally a X–2LO line at 500.5 nm. At a temperature of $T = 42$ K, the lines of bound excitons almost disappear, the free exciton emission dominates the spectrum and the lines X–LO, X–2LO show the characteristic asymmetry described by relations (7.12) and (7.13). After Gross *et al.* [10]. (b) Comparison of the experimental lineshape X–LO, solid line, with the theoretical one (7.12), dashed line. Crystal CdSe at a temperature of $T = 44$ K. After Gross *et al.* [12].

In order to answer this question, a short excursion into the irreducible representations of point groups will be of use [3, 13]. Let Γ^α, Γ^β, Γ^μ be the irreducible representations (in general, of three different point groups of symmetry), corresponding to the wavefunction of the initial and final electron states and to the matrix element operator of the corresponding optical transition, respectively. Matrix elements of the type $\langle\Gamma^\beta|\Gamma^\mu|\Gamma^\alpha\rangle$ are then non-zero (i.e. the transition is allowed) if and only if

$$\text{the direct product}(\Gamma^\alpha \otimes \Gamma^\mu)\text{includes}\Gamma^\beta \tag{7.14a}$$

or, equivalently,

$$\text{the direct product}(\Gamma^\alpha \otimes \Gamma^\beta \otimes \Gamma^\mu)\text{includes a fully symmetric representation}\Gamma_1. \tag{7.14b}$$

Next, by using (7.14), we shall find the selection rule concerning LO-phonon participation in the excitonic luminescence of a commonly occurring hexagonal wurtzite modification of CdS crystals. Let us denote as **c** the six-fold rotation axis of the highest symmetry. The band structure is schematically shown in Fig. 7.12. The corresponding point group of crystal symmetry is C_{6v}.

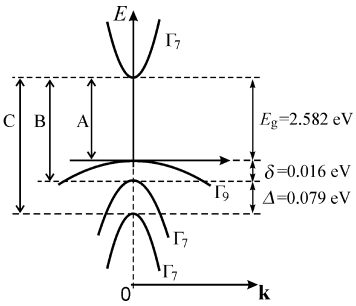

Fig. 7.12
Schematic of the energy band structure of hexagonal wurtzite CdS crystals. Δ stands for the spin–orbit splitting and δ is the splitting of the highest valence band by the crystal field. The transitions between three valence bands and the conduction band are usually marked as A, B, C. The emission lines in Fig. 7.11 belong to the A transitions.

Because the spin–orbit splitting of the valence band at the Γ point plays an important role here, irreducible representations of the double group are used for labelling the symmetry of the electron states. Let us first study the onset of the absorption edge $\Gamma_9 \rightarrow \Gamma_7$, neglecting for a while the exciton states.

The CdS crystals have a direct bandgap. In the relevant notation, the highest valence band maximum at $\mathbf{k} = 0$ has a symmetry $\Gamma^\alpha = \Gamma_9$, and the conduction band minimum at the same value of $\mathbf{k}$ has a symmetry $\Gamma^\beta = \Gamma_7$. In crystals with the point group C_{6v}, the photon operator for light polarization $\mathscr{E} \perp \mathbf{c}$ (in the dipole approximation) transforms according to the irreducible representation $\Gamma^\mu = \Gamma_5$. If we calculate the direct product $\Gamma^\alpha \otimes \Gamma^\mu = \Gamma_9 \otimes \Gamma_5$ employing the character tables of the irreducible representations (or we may consult previously published multiplication tables [3]), we obtain $\Gamma_9 \otimes \Gamma_5 = \Gamma_7 \oplus \Gamma_8$. This product contains the representation $\Gamma_7 (= \Gamma^\beta)$ and, according to (7.14a), this means the interband transitions in the vicinity of the absorption edge are dipole allowed.[5]

Finally, let us pursue the luminescence of excitons with phonon participation. Because the interband transitions are dipole allowed, the exciton envelope function must be s-like ($\lambda = 0$) with a full Γ_1 symmetry. Therefore, the initial electronic state of the transition is

$$\Gamma^\alpha = \Gamma_1 \otimes \Gamma_7 \otimes \Gamma_9 \tag{7.15}$$

(i.e. a free exciton), the final state being the crystal ground state $|0\rangle$, which is certainly spherically symmetric: $\Gamma^\beta = \Gamma_1$. The overall operator of the transition matrix element transforms like $\Gamma^\mu = \Gamma_{\text{photon}} \otimes \Gamma_{\text{phonon}} = \Gamma_5 \otimes \Gamma_{\text{phonon}}$. In CdS, the LO-phonon has an energy of $\hbar\omega_0 = 37\,\text{meV}$ and symmetry Γ_5. Taking into consideration (7.15) and using the multiplication table we therefore obtain

$$\begin{aligned}\Gamma^\alpha \otimes \Gamma^\beta \otimes \Gamma^\mu &= (\Gamma_1 \otimes \Gamma_7 \otimes \Gamma_9) \otimes \Gamma_1 \otimes (\Gamma_5 \otimes \Gamma_5) \\ &= (\Gamma_7 \otimes \Gamma_9) \otimes (\Gamma_5 \otimes \Gamma_5) \\ &= (\Gamma_5 \oplus \Gamma_6) \otimes (\Gamma_1 \oplus \Gamma_2 \oplus \Gamma_6) \\ &= \Gamma_1 \oplus \Gamma_2 \oplus \Gamma_3 \oplus \Gamma_4 + 3\Gamma_5 + 3\Gamma_6.\end{aligned}$$

From the last expression it is evident that the product $\Gamma^\alpha \otimes \Gamma^\beta \otimes \Gamma^\mu$ includes Γ_1, therefore, according to condition (7.14b), the corresponding transition is allowed. The LO-phonon assisted radiative recombination of free excitons in crystals of CdS type is thus allowed by the selection rules.

We shall close this subsection with a brief summary: The participation of optical phonons in free exciton radiative annihilation in direct semiconductors removes polariton effects and leads to the appearance of luminescence lines with a characteristic shape described by relations (7.12) and (7.13). Their intensity dependence is linear in a wide range of excitation intensities. Prominent participation of LO-phonons in exciton luminescence, which cannot be overlooked particularly in II-VI materials, follows from the fact that these phonons have in polar semiconductors the strongest coupling—Fröhlich

[5] Sometimes the term 'first-class dipole-allowed' direct transitions is used; see the book by Peyghambarian, N., Koch, S. W., and Mysyrowicz, A. (1993), *Introduction to Semiconductor Optics*. Prentice Hall, Englewood Cliffs N.J.

coupling—with excitons (Section 4.2). In I-VII semiconductors, which are even more polar, the LO-phonon assisted luminescence of free excitons also occurs (for example in CuCl), but some of them have an indirect bandgap (AgBr, TlBr) and the mechanism of exciton luminescence is rather different there; we will explain this now.

7.1.4 Luminescence of free excitons in indirect-bandgap semiconductors

The first important fact affecting quite essentially (and basically in a positive sense) luminescence processes in indirect-bandgap semiconductors is the absence of polariton states. This is documented in Fig. 7.13. The energy minimum of the exciton states is located at the $\mathbf{K}_i$, a point sufficiently distant from $|0\rangle$ and the exciton and photon dispersion curves therefore do not cross each other. This phenomenon markedly simplifies the discussion of exciton luminescence in these materials.

A second important factor, following from the very nature of the indirect bandgap and also from Fig. 7.13, is the indispensability of participation of non-zero $\mathbf{q}_{\text{phonon}} \cong \mathbf{K}_i$ phonons in the radiative recombination process. This is, as we already know, a positive aspect—it enables the whole population of free excitons to recombine radiatively because a suitable 'recoil phonon' provides the momentum mismatch $\sim \hbar\mathbf{K}_i$. This time, however, the approximate equality $\mathbf{q}_{\text{phonon}} \cong \mathbf{K}_{\text{exc}}$ is no longer valid, unlike the case of a direct semiconductor. The reason for this consists in the fact that the $\mathbf{K}_i$ point is *de facto* in all known indirect semiconductors situated at the first Brillouin zone boundary or in its close vicinity, thus $|\mathbf{q}_{\text{phonon}}| \cong |\mathbf{K}_i| \gg |\mathbf{K}_{\text{exc}}|$, as indicated in Fig. 7.13. In this case, as we discussed in the preceding section, the probability $W^{(1)}$ of phonon creation does not depend on $\mathbf{q}_{\text{phonon}}$, and it follows immediately from eqn (7.11) that the spectral lineshape of the one-phonon assisted free exciton luminescence will reflect exactly the Maxwell–Boltzmann distribution of exciton kinetic energies. Now we can rewrite expression (7.11) as

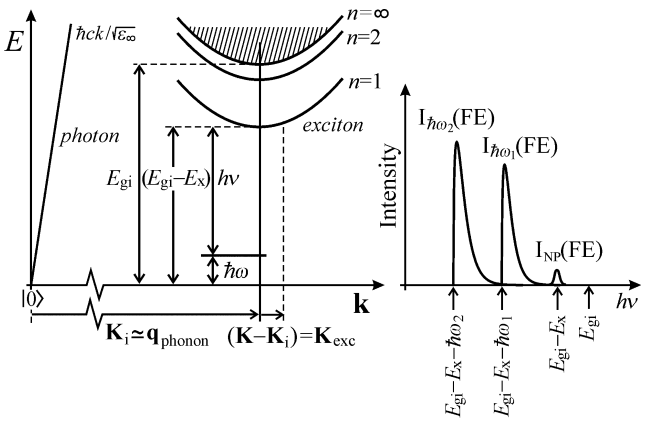

Fig. 7.13
Dispersion curves of a free exciton and a photon in an indirect-bandgap semiconductor. The polariton states do not exist. On the right: schematic of the exciton luminescence spectrum (I_{NP} stands for a no-phonon line).

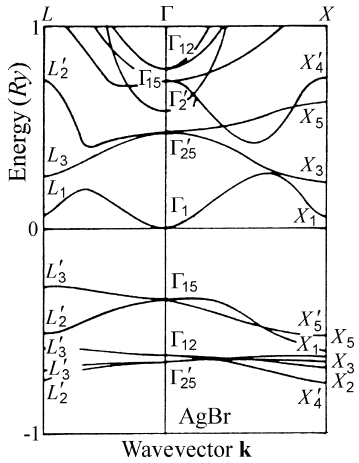

Fig. 7.14
Band structure of AgBr. The valence band maximum at the L point has a symmetry L_3', and the conduction band minimum with a symmetry Γ_1 is located at the Brillouin zone centre (Γ point, $\mathbf{k} = 0$). An ion of Br^- is placed at the origin of the coordinate system. Energy is plotted in units of $Ry(H) \approx 13.6\,eV$. After Kunz [14].

$$I_{sp(i)}^{(1)}(h\nu) \cong (h\nu - [(E_{gi} - E_X) - \hbar\omega])^{1/2} \exp - \frac{h\nu - [(E_{gi} - E_X) - \hbar\omega]}{k_B T}, \tag{7.16}$$

where the index (i) indicates the indirect bandgap. Appendix B features in detail the way in which the shape (7.16) or (7.12) can be modified in experiment by the influence of a finite slit width of the spectral apparatus and by so-called phonon broadening.

What remains to be considered is what kind of a phonon will take part in the recombination process. In strongly polar crystals of AgBr one would *a priori* expect participation of an LO-phonon. Surprisingly, this is not the case (that is why we have also omitted the index (0) in the phonon energy $\hbar\omega$ in (7.16)). Why?

Selection rules arising from the symmetry of phonon and electron states will apply, analogously to Subsection 7.1.3. Crystals of AgBr have a cubic structure belonging to the point group O_h. The valence band maximum is situated at the boundary of the first Brillouin zone and has a L_3' symmetry, while the conduction band minimum is at the Brillouin zone centre and has a Γ_1 symmetry (see Fig. 7.14) [14]. A photon in the crystal structure O_h transforms according to the irreducible representation Γ_{15}. (Relativistic effects and thus the spin–orbit splitting of the highest valence state in AgBr can be disregarded; thus the electronic states are classified according to a single point group.) Considering the symmetry of the exciton envelope to be Γ_1, the initial state of the transition related to the exciton recombination has a symmetry $\Gamma^\alpha = \Gamma_1 \otimes \Gamma_1 \otimes L_3'$. The crystal ground state Γ_1 represents the transition final state Γ^β (thus $\Gamma^\beta = \Gamma_1$), and the transition matrix element belongs to the representation $\Gamma^\mu = \Gamma_{photon} \otimes L_{phonon} = \Gamma_{15} \otimes L_{phonon}$. Then, in accordance with (7.14a), the direct product

$$(\Gamma^\alpha \otimes \Gamma^\mu) = (\Gamma_1 \otimes \Gamma_1 \otimes L_3') \otimes (\Gamma_{15} \otimes L_{phonon}) = L_3' \otimes \Gamma_{15} \otimes L_{phonon} \tag{7.17}$$

must contain $\Gamma^\beta = \Gamma_1$ if the phonon-assisted transition is to be allowed.

Because L_3' and Γ_{15} are odd representations, L_{phonon} must be an even representation if the direct product (7.17) is to contain an even (Γ_1) representation. At the L point, AgBr has two types of phonons transforming according to an even representation: L_1(LA) and L_3(TO), see Fig. 4.6 (and also Problem 4/4).

We perform the multiplication indicated in (7.17), using the tables of irreducible representations of points with symmetries L and Γ [13], for both types of phonons in question:

phonon L_1:

$$\begin{aligned}(L_3' \otimes \Gamma_{15}) \otimes L_1 &= L_3' \otimes (\Gamma_{15} \otimes L_1) = L_3' \otimes (L_1' \oplus L_3') \\ &= \Gamma_1 \oplus \Gamma_2 \oplus 2\Gamma_{12} \oplus 3\Gamma'_{25} \oplus 3\Gamma'_{15}, \end{aligned} \tag{7.18a}$$

phonon L_3:

$$\begin{aligned}(L_3' \otimes \Gamma_{15}) \otimes L_3 &= L_3' \otimes (\Gamma_{15} \otimes L_3) = L_3' \otimes (L_1' \oplus L_2' \oplus 2L_3') \\ &= 2\,(\Gamma_1 \oplus \Gamma_2 \oplus 2\Gamma_{12} \oplus 3\Gamma'_{25} \oplus 3\Gamma'_{15}). \end{aligned} \tag{7.18b}$$

Indeed, both eqns (7.18a) and (7.18b) contain Γ_1 on their right side, therefore the participation of both the L_1(LA) and L_3(TO) phonons in the radiative recombination of an indirect free exciton in AgBr is allowed. On the contrary, the LO-phonon in AgBr has symmetry L_2' at the L point and therefore its participation in the exciton luminescence is forbidden.

Selection rules derived in this way are in perfect agreement with experiment [15], as documented in Fig. 7.15. The dominant line in the low-temperature edge emission of pure AgBr crystals is a TO(L)-phonon replica of free exciton luminescence (I_{TO}(FE)),[6] and, in addition, also a markedly weaker line I_{LA}(FE) is present. This is due to the higher density of states of the TO-phonons in the L point along with a stronger coupling of these phonons with excitons over that of TA-phonons. In Fig. 7.15, also the theoretical lineshape (7.16) calculated using $\hbar\omega_{TO} \cong 8\,\text{meV}$, $\hbar\omega_{LA} \cong 12\,\text{meV}$ and an effective temperature of $T = 10\,\text{K}$ is depicted (symbols; the height of the theoretical curves is always normalized to the maximum of the measured line). Agreement between theory and experiment, as far as the lineshape is concerned, appears also to be very good. We point out the characteristic asymmetry towards higher photon energies. In this context, we refer the reader also to Fig. 8.20.

Figure 7.15 contains another two interesting pieces of information. Firstly, also a weak line I_{NP}(FE) corresponding to the radiative recombination of an indirect free exciton without phonon participation is present. This process is theoretically forbidden in an ideal periodic lattice, however, due to the presence of residual impurities and lattice defects breaking the strictly periodic arrangement of atoms, it becomes partially allowed. Secondly, these residual impurity atoms manifest themselves in the luminescence spectrum very distinctly: free excitons get localized at the impurities, creating bound excitons (BE) which also decay radiatively. The corresponding lines are, contrary to free exciton luminescence, of extrinsic origin and this is reflected in their labelling: EX_{TO}(BE), EX_{LA}(BE). It is expected that in this case the intensity ratio $I_{TO}(FE)/EX_{TO}(BE)$ varies significantly from sample to sample.

In silicon and germanium, similar symmetry-driven selection rules apply like in the case of AgBr. It turns out that in phonon-assisted free exciton radiative recombination in silicon all types of phonons (LO, TO, LA, TA) are allowed. Experimentally, though, only three lines I_{TA}(FE), I_{LO}(FE) and I_{TO}(FE) are observed, as can be seen in Fig. 1.1. The reason for this consists in the degeneration of the LA, LO phonon dispersion curves at the X point of the Brillouin zone (Fig. 4.3), in the close vicinity of which the conduction band minimum in silicon is situated (Fig. 7.16). The weak I_{LA}(FE) line thus *de facto* merges with the I_{LO}(FE) line. In germanium, two allowed free exciton luminescence lines, namely I_{LA}(FE) and I_{TO}(FE), are observed, again in accord with the selection rules. Here, the spectral lineshape is more complicated due to the exciton ground state splitting (interaction of the anisotropic conduction band minima with degenerate hole states) and non-parabolicity of the density of states. If the theoretical description of the lineshape (7.13) is to be used to fit exactly the experiment, it needs substantial corrections. Further information on this issue can be found in [16, 17].

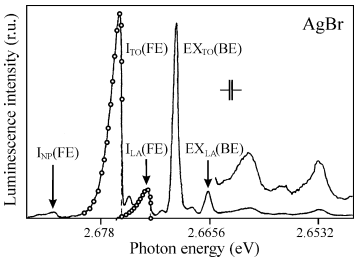

Fig. 7.15
Photoluminescence edge emission spectrum of pure AgBr (residual impurities ≤ 1 ppm) at a bath temperature of $T = 4.2\,\text{K}$. Starting from the highest photon energy: a line of no-phonon recombination of a free exciton I_{NP}(FE), a TO-phonon I_{TO}(FE) and LA-phonon I_{LA}(FE) assisted luminescence of a free exciton, respectively. Normalized emission lineshapes, calculated using (7.16) with an effective temperature of 10 K, are denoted by circles. (Compare with Fig. 7.13.) The EX_{TO}(BE) and EX_{LA}(BE) lines originate in the radiative annihilation of an exciton bound to an unknown residual impurity. The last three weak lines are two-phonon replicas. After von der Osten and Weber [15].

[6] This labelling is sometimes used in order to stress the intrinsic (I) character of the free exciton (FE) emission.

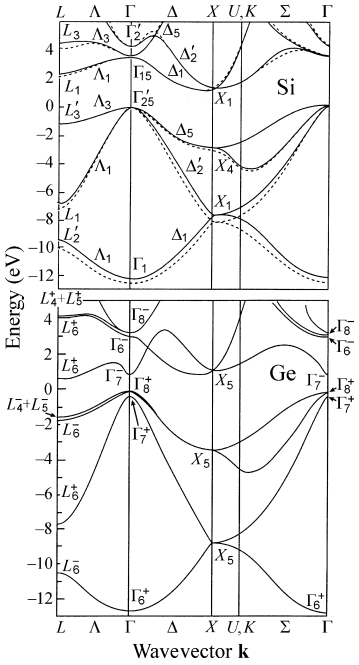

Fig. 7.16
Band structure of Si and Ge. In silicon, an indirect forbidden gap $E_{gi} \cong 1.17\,\text{eV}$ is formed between the top of the valence band (Γ'_{25}) and the conduction band minimum situated along the Δ line, close to the X_1 point. In germanium, there is an indirect bandgap $\Gamma_8^+ - L_6^+$ of the magnitude of $E_{gi} \cong 0.745\,\text{eV}$. Because Ge is heavier than Si, the spin–orbit splitting of the valence band maximum is more distinct and a double group notation is used for labelling the symmetry of the electronic states.

Finally, one important note: Similarly to the case of (X − *m* LO) lines (Section 7.1.3), a significant additional guideline to identify various free exciton luminescence lines in indirect semiconductors is their linear dependence on pump intensity.

We shall close this subsection by stressing once more what has already been mentioned repeatedly: a single microscopic luminescence centre in an indirect-bandgap semiconductor may manifest itself through several emission lines of comparable intensities (phonon replicas).

7.2 Bound excitons

We have already noted that lattice defects, and especially impurity atoms, present in the crystal either intentionally (doping) or as residual impurities which the preparation technology fails to get rid off, make very efficient potential wells—traps—for free excitons. The exciton loses its kinetic energy owing to localization at these traps and such excitons are then called *bound excitons* (BE), to be distinguished from free excitons (FE).[7] Afterwards, a radiative or non-radiative recombination of the bound exciton, accompanied in the former case by emission of a characteristic luminescence photon, occurs again. It is a typical *extrinsic luminescence*.

As a rule, the efficiency of the bound exciton luminescence is substantially higher than that of free excitons. Emission spectra of medium-level doped or sometimes also nominally pure semiconductors are usually dominated by the bound exciton luminescence. Why? Two reasons are of importance.

1. First of all, it is the large radius of the Wannier exciton a_X itself, representing in this context a large capture cross-section σ_X for capturing of an exciton at the potential well ($\sigma_X \approx \pi a_X^2 \approx 10^{-12}\,\text{cm}^2$ if we consider a typical Bohr radius $a_X = 5\,\text{nm}$). Let us estimate the mean free exciton lifetime τ_{tr} before trapping. Obviously, it is expected that the higher the cross-section σ_X, the higher the impurity concentration N and the faster the free exciton movement, the smaller is τ_{tr}:

$$\tau_{tr} \approx \frac{1}{\sigma_X N v}, \tag{7.19}$$

where v is the thermal velocity of exciton diffusion through the lattice. Let us assume $N = 10^{15}\,\text{cm}^{-3}$ (corresponding to a nominally pure semiconductor, except silicon perhaps, where purity of $N \leq 10^{11}\,\text{cm}^{-3}$ can be reached), $\sigma_X = 10^{-12}\,\text{cm}^2$ and $v = 10^6\,\text{cm/s}$ (corresponding to a temperature of approximately 2 K); from (7.19) we obtain $\tau_{tr} \approx 10^{-9}\,\text{s}$.

This value of τ_{tr} is comparable with the radiative recombination lifetime τ_r in direct-bandgap semiconductors. This means the chance of a free exciton in such a semiconductor to emit its characteristic luminescence is roughly the same as that of being trapped at an impurity and then to recombine with emission of BE luminescence.

[7] In the case of exciton localization at an impurity atom, the term 'bound exciton' is in fact synonymous with the term 'excited state of the impurity atom'.

In an indirect-bandgap semiconductor $\tau_r \geq 10^{-4}$ s holds, thus we get $\tau_{tr} \ll \tau_r$. Therefore, the chance of a free exciton to be trapped, forming in this way a bound exciton, is far higher than to recombine radiatively with emitting the characteristic free exciton luminescence ($h\nu \approx E_{gi}–E_X–\hbar\omega$). This simple estimate implies immediately that the low-temperature free exciton luminescence—for instance in silicon at a doping level of the order of 10^{15} cm^{-3}—should not appear at all. Indeed, Fig. 1.1 corroborates this conjecture: The bottom spectrum (C) originates in a sample with a total concentration of boron and arsenic atoms of approximately 8×10^{15} cm^{-3} and it is evident that the free exciton lines $I_{TO}(FE)/I_{LO}(FE)$ at $\sim$ 1130 nm and $I_{TA}(FE)$ at $\sim$ 1090 nm (i.e. the intrinsic emission) are totally missing, while the extrinsic emission of excitons localized at boron atoms (e.g. $B_{TO}(BE)$, $B_{LO}(BE)$) is very intense. We will return to this point in more detail in Subsections 7.2.1 and 7.2.2.

2. The bound exciton luminescence is characterized by the so-called 'giant oscillator strength', as shown by Rashba and Gurgenishvili [18]. In principle this means that all the unit cells inside a 'volume' of approximately $\sim a_X^3$ around the impurity atom or defect contribute to the radiative recombination of the bound exciton. The probability of this radiative recombination (and, consequently, the relevant oscillator strength f) is thus increased by several orders of magnitude, and the radiative lifetime $\tau_r \sim 1/f$ decreases proportionally.

These two effects can also be expressed in the following way: The crystal lattice, serving as a 'matrix' for impurity atoms or defects, plays, during photoluminescence processes, the role of an 'antenna' that 'harvests' the excitation radiation and transfers the excitation energy efficiently—with the help of the motion and trapping of free excitons—to the extrinsic luminescence centres. Expressed concisely, photoluminescence is a very sensitive tool to study impurities and defects in semiconductors.

How do we identify the bound exciton luminescence in the emission spectrum? One deals with a localized excitation, characterized very often (but not always!) by a small Huang–Rhys factor. This is owing to the large radius of a typical bound exciton, or owing to the fact that the excited area is spread in the host lattice over a considerable volume. Therefore, the spectra are composed of very narrow emission lines (FWHM of the order of 0.1 meV) which, moreover, do not broaden with increasing temperature (because the bound exciton lacks kinetic energy). Figure 7.17 represents the first emission spectrum of a bound exciton published in 1960 [19], which clearly demonstrates these characteristic features. A very narrow $As_{TO}(BE)$ line originates in the TO-phonon assisted radiative recombination of an exciton bound to an arsenic atom (donor impurity in silicon). Its narrow width contrasts sharply with the neighbouring free exciton line $I_{TO/LO}(FE)$, broadened considerably at the experimental temperature of $T = 25$ K. A narrow no-phonon line of the bound exciton $As_{NP}(BE)$ is also present.

There are two additional important features contributing to the reliable identification of the extrinsic bound exciton luminescence. The first one is the

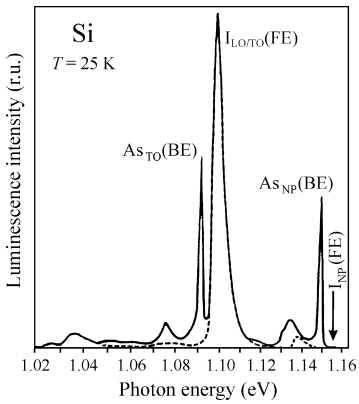

Fig. 7.17
The first published emission spectrum of a bound exciton: crystalline silicon containing an arsenic impurity with a controlled concentration of 8×10^{16} cm^{-3} (full line) in comparison with a silicon sample containing negligible concentration of impurities (dashed line). Silicon doped with arsenic shows a new line $As_{TO}(BE)$ due to radiative decay of excitons bound to As atoms. An intense $I_{LO/TO}(FE)$ line is a fingerprint of the free exciton luminescence; $As_{NP}(BE)$ denotes no-phonon emission of the bound exciton. After Haynes [19].

linear intensity dependence with the expected tendency to *saturation* at higher excitation power densities, as outlined in Section 3.5. Next, the specific spectral position of the bound exciton line may be considered to be the second feature. Because the free exciton during its localization hands over part of its energy to the surroundings (and the rest is later emitted), the bound exciton emission line must be shifted—with respect to the corresponding free exciton replica—towards *lower photon energies*. This is clearly demonstrated in Fig. 7.17. In the next subsections we shall explain in more detail the physical origin of this energy shift.

7.2.1 Excitons bound to shallow impurities

Shallow donors and acceptors, controlling in a principal way the electric conductivity of semiconductors, are of fundamental importance in semiconductor technology. These impurities can reveal themselves in a characteristic way also in luminescence radiation; this is naturally profitable because it enables the donors and acceptors to be investigated also by optical means. We shall point to the slightly different luminescence behaviour of excitons bound to ionized donors or acceptors, and that of excitons bound to these impurities in a neutral state.

Excitons bound to ionized donors (D^+–X) or acceptors (A^-–X)

This is the simplest type of bound exciton. To describe the processes of free exciton capture and subsequent radiative annihilation of the bound exciton, it is advantageous to use quantum-chemistry notation. Let us thus denote

e ..... electron,
h ..... hole,
$\oplus e$ ..... neutral donor; also D^0,
$\ominus h$ ..... neutral acceptor; also A^0,
FE ..... free exciton,
$\oplus$ ..... ionized donor; also D^+,
$\ominus$ ..... ionized acceptor; also A^-,
$\oplus\, eh$ ..... exciton bound to ionized donor; also (D^+–X) or (D^+, X),
$\ominus\, eh$ ..... exciton bound to ionized acceptor; also (A^-–X) or (A^-, X),
$\oplus\, eeh$ ..... exciton bound to neutral donor; also (D^0–X) or (D^0, X),
$\oplus\, heh$ ..... exciton bound to neutral acceptor; also (A^0–X) or (A^0, X).

The capturing event of a free exciton by an ionized donor can be described schematically as

$$\oplus + \mathrm{FE} \rightarrow \oplus\, eh + D_1, \tag{7.20a}$$

where D_1 is the dissociation or binding energy of the exciton in the relevant complex. It is thus the energy released by the exciton during localization or, alternatively, the energy required to tear the exciton off the ionized donor and make it free again, i.e. the energy necessary to start the reaction (7.20a) going in the opposite direction. (D_1 is not to be confused with the binding energy E_X of an electron–hole pair in a free exciton!) The radiative decay of such a bound

exciton $\oplus eh$, resulting in emission of a photon $h\nu_{\mathrm{BE}}$, then reads

$$\oplus eh \rightarrow \oplus + h\nu_{\mathrm{BE}}. \tag{7.20b}$$

By combining both eqns (7.20) we obtain immediately

$$h\nu_{\mathrm{BE}} = \mathrm{FE} - D_1 \cong (E_{\mathrm{g}} - E_{\mathrm{X}}) - D_1, \tag{7.21}$$

where the meaning of the spectral shift of the bound exciton line is clear, i.e. the energy separation between the low-energy threshold of the free exciton line and the maximum of the bound exciton line is equal to the dissociation (binding) energy D_1 of the exciton at the impurity. Luminescence measurements therefore provide a simple way to find out this crucial parameter via optical experiments. Among others, this is important also because theoretical calculations are not able to cope with D_1 completely.

The problem of fundamental importance related to excitons bound to ionized impurities concerns their existence depending on the ratio of the effective masses of the carriers $\sigma = m_{\mathrm{e}}/m_{\mathrm{h}}$. It appears that neither (D^+–X) nor (A^-–X) can exist (i.e. be a stable complex) at arbitrary values of σ. The following qualitative consideration may help us to unravel this claim. In order for the exciton bound to an ionized donor $\oplus eh$ to be stable, it is required that the hole is sufficiently heavy (has small kinetic energy), otherwise it will break away from the neutral remainder $\oplus e$. In other words, the kinetic energy of the hole will surmount the gain in potential energy accomplished during localization of the exciton and the complex (D^+–X) will disappear. The theoretical dependence of the dissociation energy D_1 on σ is shown qualitatively in Fig. 7.18. It is seen that there exists a critical ratio $\sigma_{\mathrm{c}} \cong 0.43$ and the complex (D^+–X) is stable only for $\sigma \leq \sigma_{\mathrm{c}}$. Similar consideration can be repeated also for an exciton bound to an ionized acceptor (A^-–X); merely the electron and hole exchanging their roles. Such an exciton will thus be stable for $\sigma > 1/\sigma_{\mathrm{c}} \approx 2.33$, as is also shown in Fig. 7.18. (In reality, theoretical computations of the complex stability calculate, in analogy with a H_2^+ molecular ion, a slightly different dissociation energy, namely, the energy needed to break away only a hole, thus a neutral donor remains there, or only an electron, when a neutral acceptor remains.) A more detailed discussion can be found, e.g. in [20].

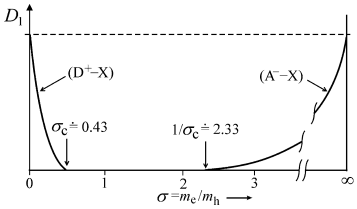

Fig. 7.18
Qualitative illustration of the dissociation energy of an exciton bound to an ionized donor (acceptor)—i.e. the energy needed to tear the free exciton off the complex—as a function of the effective masses ratio $\sigma = m_{\mathrm{e}}/m_{\mathrm{h}}$. The exciton at an ionized donor (D^+–X) may exist only for $\sigma \leq \sigma_{\mathrm{c}} \cong 0.43$, the exciton at an ionized acceptor (A^-–X) only for $\sigma > 1/\sigma_{\mathrm{c}} \cong 2.33$.

Several interesting consequences can be extracted from the above exposition:

(a) In a given material, there cannot exist simultaneously both (D^+–X) and (A^-–X).
(b) The existence of (A^-–X) in general is very unlikely because, as a rule, the hole is usually heavier than the electron ($\sigma < 1$).
(c) In silicon ($\sigma \cong 0.61$), no excitons bound to ionized impurities can exist at all, neither (D^+–X) nor (A^-–X). This is illustrated for instance in Fig. 1.1; lines of this origin occur in none of the three panels.
(d) In GaAs ($\sigma \cong 0.11$) and InP ($\sigma \cong 0.0944$) we find $\sigma < \sigma_{\mathrm{c}}$, therefore the ($\mathrm{D}^+$–X) exciton should exist in these materials, unlike the (A^-–X) one. Also this conclusion is confirmed by experiment. The (D^+–X) line can be identified in the emission spectrum of InP shown in Fig. 7.8; this line

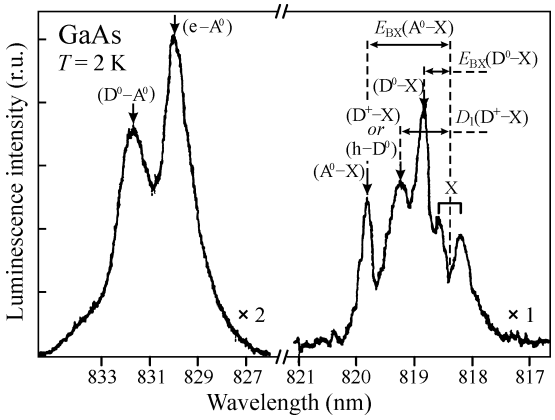

Fig. 7.19
Emission spectrum of a thin layer of GaAs (prepared by chemical epitaxy in vacuum) at a temperature of $T = 2$ K. After Bernussi *et al.* [21].

occurs also in GaAs but coincides spectrally with the (h–D^0) line (see, e.g., Figs 7.6 and 7.19 [21]). No line which could be attributed to (A$^-$–X) occurs in the mentioned figures.

Excitons bound to neutral donors (D^0–X) or neutral acceptors (A^0–X)

Numerous theoretical computations and experiments have shown that excitons bound to a neutral impurity are stable at an arbitrary σ ratio. This is a substantial difference in regard to the previous case. One can speculate qualitatively about the reasons in the following way.

An exciton bound to a neutral donor $\oplus eeh$ is—in the limit of a heavy hole $\sigma \to 0$ (i.e. $m_h \to \infty$)—an analogy to the hydrogen molecule H_2, which is a very well known and stable particle with a dissociation energy (the energy necessary for decomposing H_2 into two hydrogen atoms) equal to 0.33 Ry(H) = 4.5 eV. By analogy, we can conclude that the dissociation energy E_{BX} of an exciton localized at a neutral donor will be $E_{BX} \approx 0.33\, E_D$, where E_D is the ionization energy of the relevant donor. In the opposite limit of a light hole $\sigma \to \infty$, only the electron part of the exciton is bound to the impurity, which is actually an analogy to the H^- ion. This ion is also a stable object with dissociation energy of approximately 0.055 Ry (H); the corresponding exciton binding energy will thus be $E_{BX} \approx 0.055\ E_D$. A variety of interpolations between these two limit cases exist, nevertheless, it appears that E_{BX}, despite passing through a minimum, stays permanently above zero.

To describe the creation and subsequent radiative decay of a bound exciton, equations analogous to eqn (7.20) can be written:

$$\oplus\, e + \mathrm{FE} \to \oplus\, eeh + E_{BX}, \tag{7.22a}$$

$$\oplus\, eeh \to \oplus\, e + h\nu_{BE}. \tag{7.22b}$$

By eliminating $\oplus\, eeh$ we obtain

$h\nu_{BE} = \mathrm{FE} - E_{BX} = (E_g - E_X) - E_{BX}$ (in a direct-bandgap semiconductor),

$h\nu_{BE} = \mathrm{FE} - E_{BX} = (E_{gi} - E_X - \hbar\omega) - E_{BX}$ (in an indirect-bandgap semiconductor).

The emission line of a bound exciton is thus again red-shifted by an amount equal to the binding (dissociation) energy E_{BX}.

As an example we give in Fig. 7.19 the emission spectrum of GaAs at $T = 2\,\mathrm{K}$ which, being measured in a sufficiently wide range of wavelengths, incorporates a number of lines. We have already discussed previously the origin of all of them, starting from the (D^0–A^0) band at the longest wavelengths and terminating with the polariton emission (X) on the opposite side. At this moment, let us pay attention to the (D^0–X), (A^0–X) and (D^+–X) lines. The binding energy E_{BX} of the (D^0–X) exciton is, as can be deduced from Fig. 7.19, substantially smaller than that of (A^0–X). This is understandable because m_h ($\approx 0.61\ m_0$) is significantly larger than m_e ($\approx 0.066\, m_0$). What is less understandable at first sight is why the (D^+–X) line is more distant from the free exciton line than the (D^0–X) one, or—in our notation—why $D_1 > E_{BX}$. Then, a related question arises as whether a similar relation holds universally in all materials.

The answer is: No, it does not. The relation between D_1 and E_{BX} depends strongly on the ratio σ, as demonstrated qualitatively in Fig. 7.20. The exciton bound to an ionized donor is, as noted above, a stable complex only for $\sigma < \sigma_c$; however, D_1 increases rather abruptly with further decrease of σ. On the other hand, it is true that $E_{BX} > 0$ holds for arbitrary σ but the increase in E_{BX} is rather slow with decreasing σ and both curves cross each other somewhere. Therefore, the relation between D_1 and E_{BX} is material-dependent; σ is sufficiently small in GaAs as well as in most direct semiconductors and therefore $D_1 > E_{BX}$ applies there.

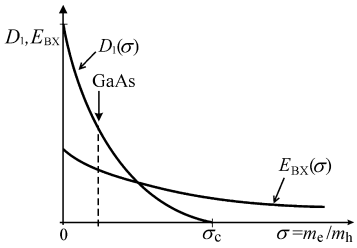

Fig. 7.20
The ratio of the binding energies of an exciton localized at an ionized (D_1) and neutral (E_{BX}) donor.

There is a very important law related to excitons bound to neutral donors and acceptors, usually referred to as *Haynes' rule*. It can be seen in Figs 7.6, 7.8 or 7.19 that the binding energy of excitons localized at acceptors differs in general from that of excitons localized at donors, as we have already discussed. Nevertheless, Haynes in 1960 found out empirically—just with the help of luminescence spectroscopy—an even more delicate relation, namely, that E_{BX} depends on the chemical nature of the donor or acceptor atom. Or, the energy E_{BX} depends (slightly) on whether the exciton is bound to an atom of, for example, phosphorus or arsenic in silicon (both the impurities being donors in silicon). Till now, we have not taken this fact into account in our exposition, in other words, we used the effective mass approximation and we were interested only in the ratio $\sigma = m_e/m_h$ of the host material, but the possible influence of the chemical nature of the impurity was disregarded. Haynes' rule thus points to the fact that the localized exciton 'feels' the chemical identity of the impurity atom and can bear witness to it via the specific energy of the emitted luminescence photon. This phenomenon is sometimes referred to as the 'central cell correction'.

The standard quantitative formulation of Haynes' rule in case of donors reads

$$E_{BX} = a + b\, E_D, \tag{7.23}$$

which, expressed verbally, tells that us the binding energy E_{BX} of an exciton localized at a neutral donor increases linearly with increasing binding energy

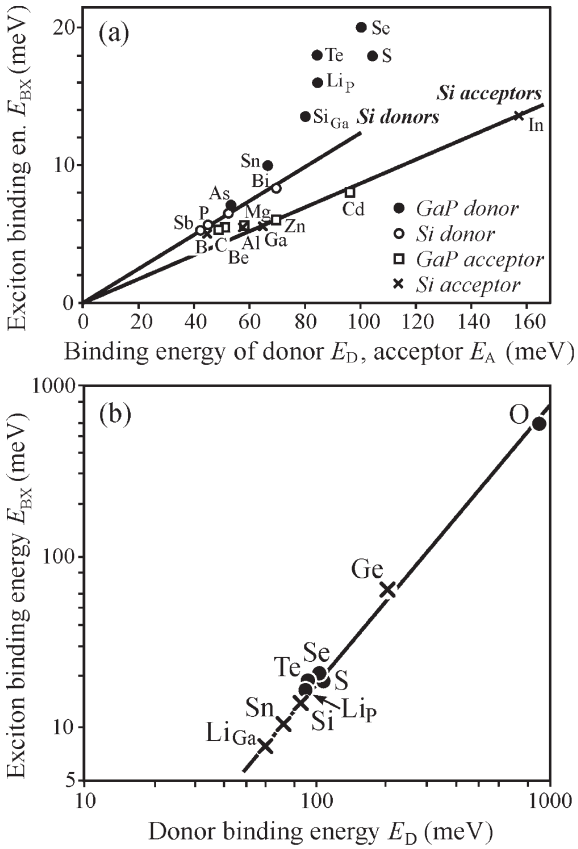

Fig. 7.21
(a) Haynes' rule: the binding energy E_{BX} of an exciton localized at a neutral impurity as a function of the binding energy of the corresponding donor (E_D) or acceptor (E_A) in Si and GaP. Full lines apply for the linear relation (7.23) in silicon. After Hayes and Stoneham [22]. (b) Modified Haynes' rule for donors in GaP: $E_{BX} \sim E_D^{1.6}$, after Herbert [24].

of the donor E_D itself. As for donors in silicon, $a = 0$ and $b \approx 0.1$, thus the binding energy of a localized exciton is approximately equal to one-tenth of the binding energy of the donor itself, which corresponds reasonably to the above mentioned estimates based on the analogy with a molecule H_2 or ion H^-. The dependence (7.23) is plotted in Fig. 7.21(a) [22]. An equation fully analogous to (7.23) holds also for the acceptors in silicon, the only difference being that there appears E_A instead of E_D and values of the constants a, b will be slightly different. A corresponding plot is also shown in Fig. 7.21(a), together with data relevant to GaP where eqn (7.23) also holds true but $a \neq 0$ and, moreover, this parameter has the opposite sign for donors and acceptors.

The simple Haynes' rule in the form of (7.23) was later explained theoretically through a chemical shift of the short-range force potential [23]. Unfortunately, this rule is not of universal validity. It turned out to be inapplicable for example to some III-V compounds such as GaAs or InP. The binding energy E_{BX} differs there for different donors and acceptors non-systematically and only very little. Therefore, if the line due to an exciton bound to a neutral donor is marked simply (D^0–X) in Figs 7.6, 7.7 or 7.19, this means that it may incorporate spectrally unresolved contributions from several donor species. A modified Haynes' rule $E_{BX} \sim E_D^{1.6}$ was proposed for GaP, as shown in Fig. 7.21(b) [24]. This modification resulted in particular from extending the

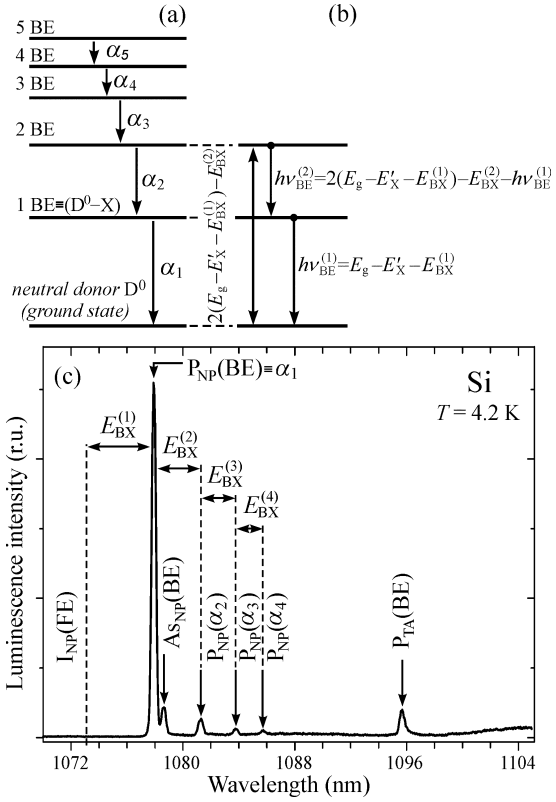

Fig. 7.22
(a) Schematic shell model of a bound multiexciton complex localized at a neutral donor. Transitions denoted α_m result from radiative decay of the mth exciton, while the exciton number in the complex decreases to $(m-1)$. (b) Energy balance for luminescence of a BMEC consisting of two bound excitons. E'_X stands for either the binding energy of the bound exciton in the case of a direct-bandgap semiconductor ($E'_X \equiv E_X$) or at no-phonon emission, or $E'_X = E_X + \hbar\omega$ for phonon replicas in a semiconductor with an indirect bandgap. (c) Low-temperature ($T = 4.2$ K) emission spectrum demonstrating the occurrence of α_1–α_4 lines in a BMEC localized at a phosphorus atom in silicon. The lines are no-phonon (NP) replicas. Also the hypothetic spectral position of a no-phonon free exciton luminescence $I_{NP}(FE)$ is depicted. Correlation with the notation used in panel (a) reads $P_{NP}(BE) \equiv \alpha_1$, $P_{NP}(\alpha_2) \equiv \alpha_2$, $P_{NP}(\alpha_3) \equiv \alpha_3$, $P_{NP}(\alpha_4) \equiv \alpha_4$. In addition to the said lines, the spectrum comprises also a weak no-phonon line $As_{NP}(BE) \equiv (D^0\text{–}X)$ originating in exciton annihilation at another neutral donor (arsenic), and also a TA-replica of luminescence of a single exciton bound at phosphorus $P_{TA}(BE)$. The silicon sample was doped by P and As to a total donor concentration exceeding 10^{16} cm^{-3}.

data in Fig. 7.21(a) to deep donors Ge and O. The validity of Haynes' rule (7.23) is also commonly not accepted in II-VI semiconductors.

Bound multiexciton complexes (BMEC)

At the beginning of the 1970s, Kaminskii and Pokrovskii discovered experimentally with the aid of luminescence spectroscopy that more than one exciton can be localized at a neutral donor or acceptor [25]. Later the term *bound multiexciton complex* (BMEC) became common to denote such objects. Here, the situation differs a bit against single excitons bound to neutral impurities (D^0–X) and (A^0–X), because the existence of (D^0–X), (A^0–X) was predicted theoretically (together with predicting the existence of excitonic molecules—Section 8.2 [26]), while the discovery of bound multiexciton complexes was, from the theoretical point of view, unexpected.

A BMEC is created in a photoexcited semiconductor in such a way that one, two, three or more excitons with step by step diminishing binding (localization) energy are successively 'wrapped around' a neutral donor D^0 or acceptor A^0. They later annihilate radiatively emitting narrow luminescence lines as depicted in Fig. 7.22(a), drawn specifically for a BMEC at a neutral donor.

If m stands for the number of bound excitons, then the energy level of the mth bound exciton is denoted as m BE ($m = 1, 2, 3, \ldots$) in Fig. 7.22.

Conformingly to previous notation 1 BE $\equiv$ (D^0–X). During the radiative annihilation of m BE, an emission line α_m arises and the number of excitons in the BMEC lowers by one (m BE $\rightarrow$ (m–1)BE). The energy balance of the multiexciton trapping and subsequent radiative recombination can be obtained by generalizing relations (7.22):

$$\begin{aligned}
&\oplus e + \mathrm{FE} \rightarrow \oplus e(eh) + E_{\mathrm{BX}}^{(1)} \\
&\oplus e(eh) - E_{\mathrm{BX}}^{(1)} + \mathrm{FE} \rightarrow \oplus e(2eh) + E_{\mathrm{BX}}^{(2)} \\
&\oplus e(2eh) - \left(E_{\mathrm{BX}}^{(1)} + E_{\mathrm{BX}}^{(2)}\right) + \mathrm{FE} \rightarrow \oplus e(3eh) + E_{\mathrm{BX}}^{(3)} \\
&\vdots \\
&\oplus e\left((m-1)\ eh\right) - \sum_{j=1}^{(m-1)} E_{\mathrm{BX}}^{(j)} + \mathrm{FE} \rightarrow \oplus e(m\, eh) + E_{\mathrm{BX}}^{(m)}. \quad (7.24a)
\end{aligned}$$

In eqns (7.24a), describing the gradual trapping of free excitons FE, $E_{\mathrm{BX}}^{(m)}$ stands for the binding energy of the mth localized exciton ($E_{\mathrm{BX}}^{(1)} \equiv E_{\mathrm{BX}}$ in our previous notation).

The radiative decay of the mth exciton leading to emission of a photon $h\nu_{\mathrm{BE}}^{(m)}$ (α_m line) proceeds in accordance with the scheme

$$\oplus e(meh) \rightarrow \oplus e\ [(m-1)\, eh] + h\nu_{\mathrm{BE}}^{(m)}, \quad (7.24b)$$

which, by means of the last equation of (7.24a), gives immediately

$$h\nu_{\mathrm{BE}}^{(m)} = \mathrm{FE} - \sum_{j=1}^{m} E_{\mathrm{BX}}^{(j)}.$$

This relation tells us that the α_m lines are shifted with respect to the position of the free exciton emission line FE (= $E_{\mathrm{gi}} - E_{\mathrm{X}} - \hbar\omega$ in an indirect-bandgap semiconductor) by a sum of binding energies of all of the localized excitons. Figure 7.22(b) illustrates the energy balance (7.24) for the $m = 1$ and $m = 2$ lines; the notation $E'_{\mathrm{X}} = E_{\mathrm{X}} + \hbar\omega$ is introduced there for brevity's sake. Considering that $E_{\mathrm{BX}}^{(m)} < E_{\mathrm{BX}}^{(m-1)}$, the α_m lines make a series densifying with increasing m. At the same time, the intensity of these lines decreases, because the number of localized excitons with higher m due to the condition $E_{\mathrm{BX}}^{(m)} < E_{\mathrm{BX}}^{(m-1)}$ decreases monotonically. This is nicely illustrated in Fig 7.22(c) which displays the low-temperature emission lines α_1–α_4 originating from a BMEC at a phosphorus atom in silicon.

The schematic displayed in Fig. 7.22(a) represents a considerably simplified version of the so-called *shell model* which was put forward by Kirczenow for explaining the luminescence in BMECs [27]. In reality, the levels in Fig. 7.22(a) are split as a result of the higher number of electron and hole states differing slightly in energy. Using a very sensitive detection system with

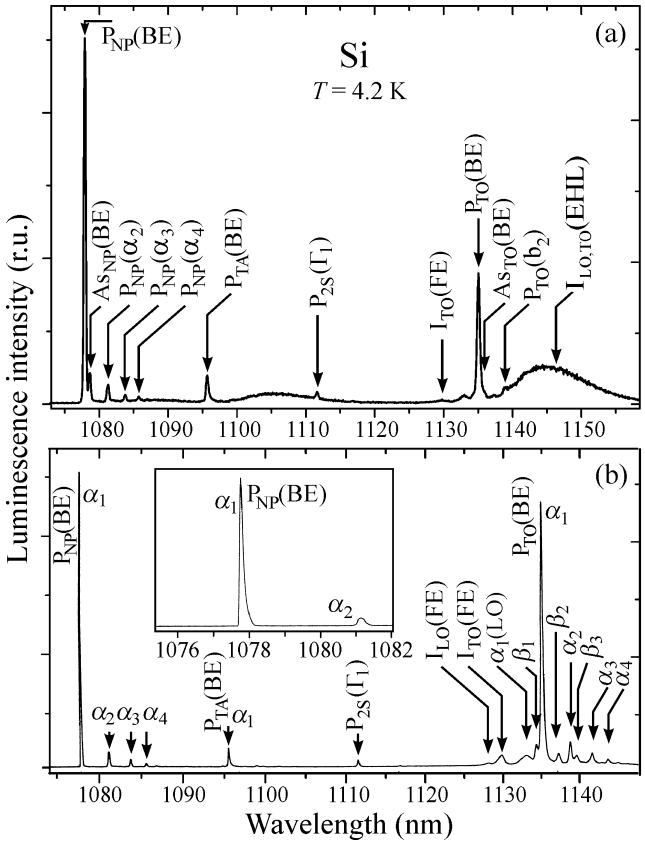

Fig. 7.23
Photoluminescence spectra of two samples of crystalline Si doped with phosphorus to approximately the same donor concentration $N_P \approx 3 \times 10^{14}\,\mathrm{cm}^{-3}$. Bath temperature $T = 4.2\,\mathrm{K}$. (a) Continuous-wave excitation 488 nm from an Ar^+-laser (excitation intensity $\sim 20\,\mathrm{W/cm}^2$), a scanning detection monochromator HRD-1 and a cooled photomultiplier with a photocathode of S1 type. After Pelant *et al.* [29]. (b) Continuous-wave excitation 514 nm from an Ar^+-laser (estimated excitation intensity $\sim 2\,\mathrm{W/cm}^2$), detection with the help of a Nicolet Fourier spectrometer with a cooled North Coast Ge detector. The inset shows the enlarged area of NP replicas. After Colley and Lightowlers [30].

a high S/N ratio, one can, in addition to the series of α_m lines, observe also weaker emission lines β_m—they can be seen for instance in Fig. 7.23(b).[8]

It is worth noting that the α_m lines in Fig. 7.22(c) represent no-phonon luminescence and, surprisingly, are more intense than the corresponding series of lines in the region of TO/LO- or TA-replicas, as one can make sure of by looking at Fig. 1.1(A) where a similar series of phosphorus-related α_1–α_4 lines occurs, too. At this point it may appear suitable to make a small deviation in a more general sense: when discussing recombination processes in indirect-bandgap semiconductors we encounter certain competition between the configurational coordinate model and the principle of quasi-momentum conservation (the configurational coordinate model was introduced in Sections 4.4 and 4.5 by assuming tacitly a direct-bandgap material). As far as silicon donors are concerned, there is a very weak exciton–phonon interaction, thus the Huang–Rhys factor is small ($S \cong 0.1$) implying that the no-phonon lumines-

[8] True values of the binding energies then differ from those of the quantities $E_{\mathrm{BX}}^{(m)}$ introduced by us, and need not satisfy the condition of monotonic decrease with increasing m. Details can be found in Thewalt, M. L. W. (1983). *Bound multiexciton–impurity complexes*. In *Excitons* (ed. E. I. Rashba and M. D. Sturge). *Modern Problems in Condensed Matter Sciences*, Vol. 2, Chap. 10. North Holland, Amsterdam.

cence lines of a localized impurity centre (phosphorus atom) are expected to be relatively intense, as indeed is observed experimentally; the first phonon replicas are substantially weaker. However, we cannot forget that in an indirect semiconductor this phenomenon is conditioned by relaxation of the quasi-momentum conservation law owing to the phoshorus-atom-induced breaking of the lattice translational symmetry. Hereby, the influence of the indirect bandgap is *de facto* annulled in this way.[9]

A similar scheme of energy levels as in Fig. 7.22 (shell model) can be introduced also in the case of a BMEC at a neutral acceptor. A corresponding series of emission lines, characteristic for a BMEC localized at boron in silicon is clearly noticeable in Fig. 1.1(C). Somewhat stronger exciton–phonon coupling in an acceptor-related BMEC causes the first phonon replicas to be more intense than no-phonon lines here. The $B_{TO}(BE)$ line, is analogous to a TO-replica of the donor α_1 line, $B_{TO}(b_1)$ corresponds to a TO-replica of the α_2 line, $B_{TO}(b_2)$ corresponds to a TO-replica of the α_3 line, etc. Fully analogous notation is used for TA-replicas in Fig. 1.1(C).

BMECs were studied in detail mainly in silicon. Lines that can be attributed to radiative decay of a BMEC were observed also in Ge, β-SiC and GaP. These are all indirect-bandgap semiconductors where the occurrence of a BMEC is quite understandable, for two reasons. First, the excitons have a relatively long lifetime in indirect semiconductors (which enhances the probability for trapping of several excitons at one centre), and second is the N-fold degeneracy of the conduction band minimum ($N = 4$ in Ge and $N = 6$ in Si) allowing up to $2N$ electrons to be placed in one molecular orbital without violating Pauli's exclusion principle. Some emission lines, observed in the direct-bandgap semiconductor GaAs, were also attributed to a BMEC; however, definitive confirmation of the existence of BMECs in these materials is missing.

The radiative recombination of various types of excitons bound to donors and acceptors represents a strong rival channel to the $(D^0–A^0)$ luminescence.

7.2.2 Quantitative luminescence analysis of shallow impurities in silicon

The utilization of low-temperature photoluminescence spectroscopy over the exciton spectral range to determine the concentration of shallow donors and acceptors in crystalline silicon was proposed in 1982 by Tajima [28]. In Table 7.2 we give the wavelengths of the luminescence lines originating in various complexes $(D^0–X)$, $(A^0–X)$ in silicon. These are TO-phonon assisted lines of excitons bound to commonly applied donors and acceptors. As will become clear hereafter, the TO-replicas are those used most frequently for the quantitative luminescence analysis of silicon.

[9] Strictly speaking, however, the presence of impurity atoms should also allow the intrinsic no-phonon luminescence of free exciton $I_{NP}(FE)$ to appear, like in AgBr, see Fig. 7.15. In spite of this, no line like $I_{NP}(FE)$ has ever been reported in silicon; this difference between AgBr and Si is probably given by the much higher concentration of both point and line defects (dislocations) in AgBr.

It follows from Table 7.2 that the spectral positions of the lines characteristic of donors and acceptors vary—according to Haynes' rule—with the chemical nature of the dopants; the variations range from fractions of nanometres to several nanometres. Such differences are in principle large enough for the individual lines to be distinguished, provided a scanning monochromator with resolving power of $R \approx 5 \times 10^3$ is used. However, if there are several types of impurities in a given sample, their lines will very probably merge together due to their natural linewidth and due to possible line broadening by the finite monochromator slit, and will form an almost irresolvable band. Any effort to identify the individual lines then would not probably attain the target. Fortunately, silicon technology is highly advanced so that a very low level of residual (introduced unintentionally) impurities—down to $10^{10}\,\mathrm{cm}^{-3}$—can be reached by zone-refining. In order to achieve the desired type and value of electric conductivity, mostly phosphorus (donor) and boron (acceptor), possibly also As, Sb, Al and Ga, are used as dopants. In practise, their concentrations usually range from $10^{12}\,\mathrm{cm}^{-3}$ to $10^{18}\,\mathrm{cm}^{-3}$ and knowledge of the exact values of the concentration is basic information for both the producers and purchasers of Si ingots and wafers.

Photoluminescence analysis enabling us to determine such a concentration in the range of approximately 10^{11}–$10^{15}\,\mathrm{cm}^{-3}$ was developed primarily for boron and phosphorus. In this concentration range—i.e. for nominally pure or weakly doped Si wafers—this technique has an important role to play in supplementing the wide range of diagnostic methods (temperature-dependent Hall effect, resistivity measurements, infrared absorption spectroscopy, etc.) being commonly applied at higher concentrations of donors and acceptors. It can be stated that photoluminescence diagnostics is nowadays the only analytic method of weakly doped Si crystals that is used routinely in practice.

The essence of the method is very simple and is based on the following use of the emission lines B_{TO}(BE), P_{TO}(BE) and I_{TO}(FE), shown for example in Fig. 1.1 or Fig. 7.23 [29, 30]. It is, undoubtedly, reasonable to assume the

Table 7.2 Spectral positions of luminescence lines (TO-replicas) due to excitons bound at various impurities in Si; $T = 4.2\,\mathrm{K}$*)

Impurity	Type	Wavelength (nm)
P	SD	1135.13
As	SD	1135.97
Sb	SD	1135.04
Bi	SD	1138.32
Li	ID	1133.74
B	SA	1134.39
Al	SA	1135.60
Ga	SA	1136.15
In	SA	1144.83
Tl	SA	1177.59
C	I	1164.36
free exciton	–	1129.76

*) SD stands for a substitutional donor, ID interstitial donor, SA substitutional acceptor, I isoelectronic impurity.

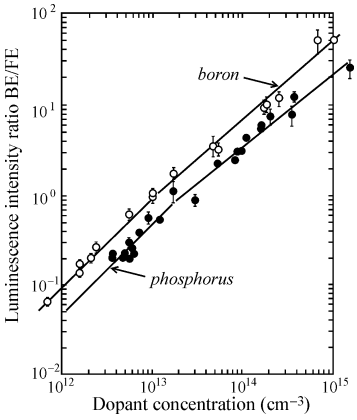

Fig. 7.24
Calibration curves for the quantitative determination of B and P concentrations in silicon from photoluminescence spectra at $T = 4.2\,\mathrm{K}$ (dependence of the ratio of intensities $P_{TO}(BE)/I_{TO}(FE)$ and $B_{TO}(BE)/I_{TO}(FE)$ on phosphorus and boron concentrations, respectively). After Pelant *et al.* [31].

intensities of the lines $B_{TO}(BE)$ and $P_{TO}(BE)$ to be proportional to the relevant concentrations of boron N_B or phosphorus N_P, respectively. On the other hand, the intrinsic emission $I_{TO}(FE)$ line, as we have already stressed several times, is characteristic of those parts of the crystal where these dopants are not present. The ratio of the line intensities $B_{TO}(BE)/I_{TO}(FE)$ or $P_{TO}(BE)/I_{TO}(FE)$ is surely an increasing function of the concentrations N_B, or N_P, respectively. If we determine experimentally this dependence (the so-called calibration curve) via luminescence measurements performed on samples with a known content of boron and phosphorus, the dopant concentrations N_B and N_P in unknown samples can then be determined easily from the relevant luminescence spectra using these calibration curves.

An example of such calibration curves is displayed in Fig. 7.24 [31]. It should be stressed that these curves—as shown—are not applicable universally because the intensity ratio of the bound to free exciton lines depends slightly on the excitation power density. Measurements of calibration curves and experimental investigation of samples in which the dopant concentration is to be determined thus have to be always performed using the same experimental setup and keeping all the experimental parameters constant. In this case, it is not even necessary to take into account spectral corrections. The calibration curves in Fig. 7.24 were obtained using the experimental set-up drawn in Fig. 2.2(a).

It is worth stressing that the measurement of intensities of the $B_{TO}(BE)$ or $P_{TO}(BE)$ lines alone is not sufficient to determine the unknown concentrations because the overall luminescence intensity is sample-dependent (being affected by surface treatment, reproducibility of the sample position with respect to the optical collecting system, etc.); it is thus always necessary to determine the ratio BE/FE. This fact then specifies the above mentioned limits of applicability of the method: in strongly doped samples (N_B, $N_P \geq 10^{15}\,\mathrm{cm}^{-3}$) the $I_{TO}(FE)$ line becomes undetectable, as clearly demonstrated in Fig. 1.1(C); in very pure samples (N_B, $N_P \leq 10^{11}\,\mathrm{cm}^{-3}$), on the other hand, the $B_{TO}(BE)$ and $P_{TO}(BE)$ lines disappear.

While the essence of the method is simple, its experimental realization is not quite trivial. There are several reasons for this. First of all, the luminescence of silicon is very weak, several orders of magnitude below that of direct-bandgap materials (GaAs). Moreover, judged from the point of view of detectors of weak photon fluxes, this luminescence is situated in a very unsuitable spectral range. As for photomultipliers, only types with an S1 photocathode are sensitive in the range 1100–1200 nm, but also for them this wavelengths represent the red limit of their sensitivity. Similar arguments can be applied as for silicon CCD detectors. It is possible to use a germanium detector, however, only special high-sensitive types with efficient noise suppression are suitable (Edinburgh Instruments, formerly North Coast). The problem is all the more difficult because it is necessary to measure the spectra with a high resolution R_{real}, therefore with a relatively narrow slit of the spectral apparatus ($\Delta\lambda = L^{-1}\Delta\ell \approx 0.25\,\mathrm{nm}$). The possibility to circumvent the mentioned difficulties by using a very intense excitation source (e.g. a pulsed laser) is also out of the question because, under strong pumping, a qualitative change

of the emission spectrum occurs—a novel broad band at ∼1143 nm labelled $I_{LO,TO}$(EHL) in Fig. 1.1 begins to prevail, whose origin, consisting in radiative recombination of an electron–hole liquid, is discussed in detail in Section 8.4. This band to a large degree masks the lines of bound excitons, particularly in very pure samples.

It is therefore necessary to choose a certain optimal level of (continuous) pumping and pay attention to the proper choice of monochromator, detector and also of efficient collection of an optical system. What follows from the above discussed difficulties is the particular choice of TO replicas for the method under discussion, because in their spectral range, both the lines originating from the impurities and the free exciton line I_{TO}(FE) are relatively intense.

This method can serve as an example to demonstrate clearly some advantages of Fourier luminescence spectroscopy. Figure 7.23 shows a comparison of (a) an emission spectrum obtained in a conventional experimental set-up [29] with (b) an emission spectrum measured by a Fourier spectrometer [30]. It becomes evident that the Fourier-measured spectrum exhibits a markedly higher *S*/*N* ratio, even under lower excitation intensity (as reflected among others in the total absence of the $I_{LO,TO}$(EHL) band). The accuracy achieved in the Fourier approach is substantially better (± 10%) compared with that obtained with a scanning monochromator (± 30%). The sensitivity in the Fourier arrangement can attain almost unbelievable levels—it enables us to distinguish safely a tiny spectral shift and fine structure in the emission lines of bound excitons in Si crystals with different content of silicon isotopes [32]! This opens further diagnostic possibilities.

Another experimental aspect deserves special attention, namely, the method of sample cooling. It is mandatory that the samples must be immersed in a cooling medium (liquid He), an optical bath He cryostat is thus a necessity. We emphasize this because there is sometimes a tendency to replace the bath cryostat by a cheaper option—a continuous flow cryostat with a closed He cycle where the cooling is mediated only by the heat transfer in He vapour. In this case, however, the cooling power is incomparably lower and the samples are strongly heated by the absorbed excitation radiation (the reader is reminded that silicon has low luminescence efficiency—the prevailing part of the excitation energy is converted, owing to non-radiative transitions, into heat!). This results in 'evaporating' bound excitons from the impurity atoms and in a corresponding increase of the free exciton concentration, which entails an appreciable drop in intensity of the B_{TO}(BE) and P_{TO}(BE) lines and, vice versa, an increase in the I_{TO}(FE) line intensity. The significance of this effect is demonstrated in Fig. 7.25 [33, 34]: upon an increase in temperature by a mere three kelvin the intensity ratio B_{TO}(BE)/I_{TO}(FE) is decreased by more than one order of magnitude! Insufficient cooling therefore leads to a rapid deterioration of the measurement sensitivity, loss of the required spectral resolution and the method finally declines in importance.

Upon introducing the photoluminescence analysis of silicon by Tajima, the method was independently developed and confirmed at several other laboratories [30, 31, 35, 36]. The results were identical as far as the principal features

were concerned, even if Colley and Lightowlers [30] proposed a modification to consider the NP replicas instead of TO ones for the bound excitons, and the TO replica to employ for free excitons only. Besides calibration curves for boron and phosphorus, they presented calibration curve also for aluminium; Schumacher and Whitney [36] in addition for gallium and Broussel *et al*. [37] for arsenic.

An effort is being made to extend similar photoluminescence diagnostics of dopants to other semiconductor materials. However, serious problems are often encountered owing either to high residual impurity concentrations or insufficient resolved lines from different donor species. Nevertheless, the determination of luminescence of shallow impurity concentrations in CdTe has been published [38] and attempts to develop characterization methods of GaAs with the help of Fourier photoluminescence and magneto-photoluminescence spectroscopy have been reported, e.g. [39].

7.2.3 Excitons bound to isoelectronic impurities

The exciton can be trapped—besides the above discussed cases of localization at ionized or neutral donors and acceptors—also at *isovalent* or *isoelectronic impurities*. By an impurity like this we understand a substitutionally built-in atom from the same group (column) of the periodic table of elements which the original constituent of the host lattice comes from. Unlike donors or acceptors, we do not encounter here a weakly bound 'extra' electron or hole that could influence the electric conductivity. Typical examples to be discussed in more detail are a nitrogen atom in place of phosphorus in GaP (GaP/N) and an iodine ion I^- substituting bromine in AgBr (AgBr/I^-). In most cases, as we shall see, the exciton bound to an isoelectronic trap presents a highly efficient channel of radiative recombination. (Also thallium activated alkali halides (KCl/Tl, CsI/Tl), often quoted in older literature as examples of efficient phosphors and scintillators, belong to a certain extent to this category [40].)

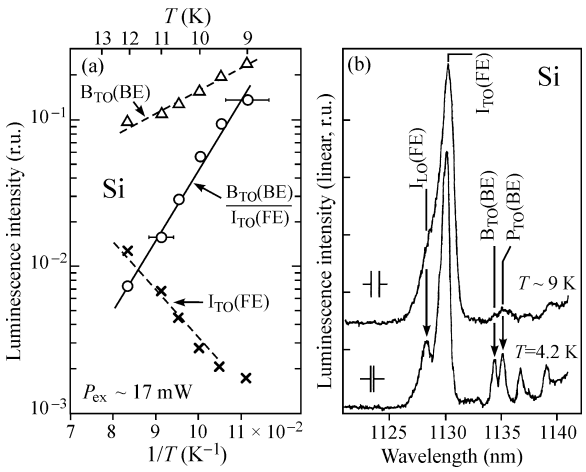

Fig. 7.25
(a) Temperature dependence of intensities of the B_{TO}(BE) and I_{TO}(FE) lines and of their ratio in silicon in the temperature range 9–12 K, measured in a continuous-flow cryostat. After Pelant *et al.* [33]. (b) Emission spectra of a very pure Si sample at $T = 4.2$ K (bath cryostat, lower spectrum) and at a nominal temperature of $T \sim 9$ K (continuous flow cryostat, upper spectrum). The spectra are normalized at 1130 nm. After Pelant *et al.* [34].

The physical mechanism of free exciton trapping is based on the electronegativity difference between the original and substituting atom. For example, a nitrogen atom N has higher electronegativity X (i.e. the ability to attract an electron) than a phosphorus atom P ($X_N = 3.0 > X_P = 2.2$). Therefore, if free photoelectrons and photoholes are created in GaP by an external excitation, the N atom may capture a nearby photoelectron with the help of short-range forces. The negatively charged N atom then attracts—now via long-range Coulomb forces—a free photohole, thereby a bound exciton localized at the nitrogen atom is created. Its radiative recombination gives a characteristic luminescence emission. Similarly, one can imagine the process to take place in AgBr crystals doped with an iodine impurity I^-; the iodine electronegativity is lower than that of bromine ($X_I = 2.7 < X_{Br} = 3.0$) and thus iodine has a higher capability to capture a photohole. A bound exciton is created again, owing to the subsequent Coulomb interaction of the positively charged centre with a photoelectron.

What is the spectral shape of the luminescence emission accompanying the recombination of an exciton bound to an isoelectronic trap? The Maxwell–Boltzmann lineshape can be certainly excluded since possible broadening due to the kinetic energy of either a free carrier or a free exciton is missing. One deals with a localized excitation; a qualitative answer can thus be obtained by applying the configurational coordinate model. It is essential in this context that the initial photocarrier capture is by short-range forces. Localization of the excitation is thus basically mediated by alteration in the occupation of the electronic shell in a single (impurity) atom. The corresponding change in the configurational coordinate $r_Q = (Q_{e0}–Q_{g0})/Q_{g0}$ (see Fig. 4.8) can then vary according to the strength of the exciton–phonon interaction. If this strength is relatively weak, which is the case of III-V semiconductors and thus also of GaP, r_Q is small (small Huang–Rhys factor $S \cong 0$) and the emission line will be narrow.

This is demonstrated in Fig. 7.26(a) where sharp lines A, B can be seen in the edge emission of a nominally pure sample of GaP [41]; both the lines are attributed to an exciton localized at a residual impurity N, being present in a concentration of $\sim 10^{15}\,\mathrm{cm}^{-3}$. The A line originates from an exciton with a total quantum number $J = 1$, the B line belongs to the exciton in the $J = 2$ state (in principle, a forbidden transition $\Delta J = 2$). The splitting is caused by the electron–hole exchange interaction; also the terms singlet and triplet exciton are often used. Both no-phonon lines and phonon replicas involving emission of optical phonons are present. (Looking at Fig. 5.10 we may find out that the lines in question are very distinct also in a GaP sample doped with Si and S.)

In strongly polar AgBr, the exciton–phonon coupling is much stronger, the surrounding host lattice reacts to the hole trapping by a sizable change of r_Q and the emission due to the iodine presence reveals itself through a broad band rather than a narrow line. The emission spectrum of the exciton localized at I^- (which is again a residual impurity in a nominally pure material, similarly to N in GaP) was already mentioned briefly in the context of our discussion of the exciton–phonon interaction (see Figs 1.2(b) and 4.10(b)). The Huang-Rhys factor S can be estimated, based on the serial number of phonon replicas located at the band maximum, to be $S = 8$–9. A similar spectrum is shown

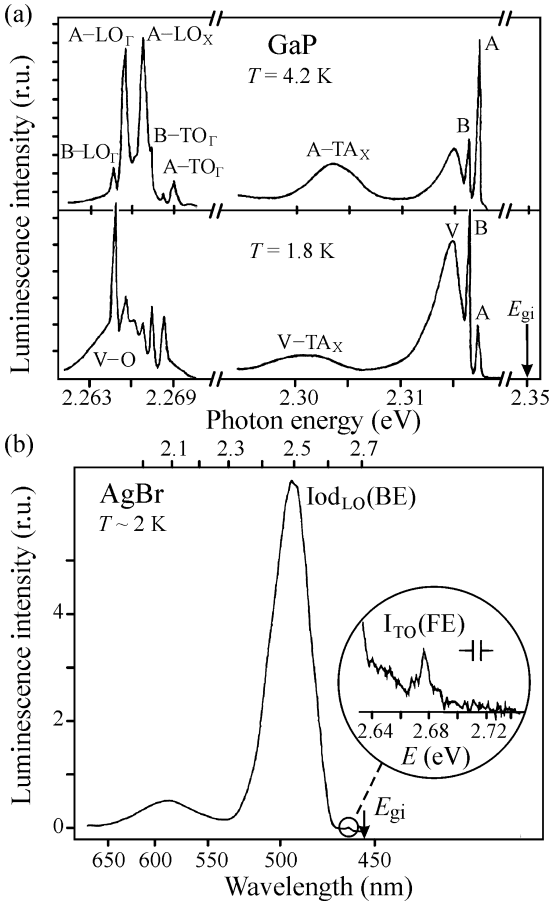

Fig. 7.26
(a) Emission spectra of nominally pure GaP under cw pumping with a dye laser 2.409 eV. The A and B lines (no-phonon ones) and their TA-, TO- and LO-phonon replicas, occurring in the edge emission range, are due to radiative decay of the excitons localized at the residual isoelectronic impurity of nitrogen ($\sim 10^{15}$ cm^{-3}). Band V originates from a similar exciton which is, moreover, influenced by the presence of distant donors and acceptors. After Gershoni *et al.* [41]. (b) Emission spectrum of nominally pure AgBr under cw pumping with a Kr^+-laser 3.53 eV. A weak indication of edge emission in the vicinity of 2.7 eV (enlarged in the circle) contains the free exciton line I_{TO}(FE). An intense broad band at $\sim$ 2.5 eV is due to an exciton bound to a residual isoelectronic impurity of iodine ($\sim 10^{16}$cm^{-3}). After Pelant [42]. The position of the indirect bandgap E_{gi} is marked. Note the different energy scales in (a) and (b).

again in Fig. 7.26(b) [42]. This figure is, however, rather exceptional in two respects. Firstly, unlike the spectra in Figs 1.2(b) and 4.10(b), the bound exciton band at ~2.5 eV lacks any fine structure. This is, however, an experimental artefact due to a not-entirely-suitable choice of the time constant of the detecting lock-in amplifier (over-damped state). On the other hand, however, this facilitated the discovery of the second—and more interesting—aspect: a weak emission of the free exciton I_{TO}(FE) at ~2.678 eV. What made recording this extremely weak line possible was just the strong noise suppression, together with a certain exceptionality of the investigated sample. The result enables us now to estimate in an illustrative way the extraordinary efficiency of the radiative recombination of excitons localized at an isoelectronic trap.

From Fig. 7.26(b), we can estimate the ratio of the spectrally integrated intensities of the bound exciton line Iod_{LO}(BE) to the free exciton line I_{TO}(BE) as $[Iod_{LO}(BE)/I_{TO}(FE)] \approx 10^4$.[10] The corresponding luminescence

[10] It is worth noticing that while the free exciton line is, owing to the strict selection rules (Section 7.1.4), accompanied by emission of TO-phonons ($\hbar\omega_{TO} \approx$ 8meV) satisfying the quasi-momentum conservation law, the fine phonon structure at the iodine band points to participation of primarily LO-phonons since separation between the individual peaks in Fig. 1.2(b) is very close to the energy of $\hbar\omega_{LO} \cong$ 16 meV. The reason is basically twofold: firstly, the free and bound

decay times found experimentally are $\tau_{\mathrm{Iod}} \approx 2 \times 10^{-5}$ s [43] and $\tau_{\mathrm{FE}} \approx 6 \times 10^{-8}$ s [44]. We write down simple relations for the intensities:

$$\mathrm{Iod_{LO}(BE)} = \frac{N_{\mathrm{Iod}}}{\tau_{\mathrm{r}}^{\mathrm{Iod}}}, \mathrm{I_{TO}(FE)} = \frac{N_{\mathrm{FE}}}{\tau_{\mathrm{r}}^{\mathrm{FE}}}, \tag{7.25}$$

where $\tau_{\mathrm{r}}^{\mathrm{Iod}}$ and $\tau_{\mathrm{r}}^{\mathrm{FE}}$ are the radiative lifetimes and N_{Iod}, N_{FE} are the concentrations of 'excited iodine ions' and of free excitons at the given pumping level, respectively. By using relation (3.3) for the luminescence efficiencies η_{Iod}, η_{FE}, we obtain from (7.25)

$$\frac{\mathrm{Iod_{LO}(BE)}}{\mathrm{I_{TO}(FE)}} = \frac{N_{\mathrm{Iod}}}{N_{\mathrm{FE}}} \frac{\eta_{\mathrm{Iod}}}{\eta_{\mathrm{FE}}} \frac{\tau_{\mathrm{FE}}}{\tau_{\mathrm{Iod}}}. \tag{7.26}$$

Now, we introduce an effective enhancement factor $z_{\mathrm{ef}} = (N_{\mathrm{Iod}}/N_{\mathrm{FE}})$ $(\eta_{\mathrm{Iod}}/\eta_{\mathrm{FE}})$ which comprises both the ratio of bound and free exciton concentrations (and thus takes into consideration the high effective cross-section of the free exciton trapping at impurity ions) and the ratio of quantum efficiencies of both the radiative processes. The factor z_{ef} then follows from relation (7.26) as

$$z_{\mathrm{ef}} = \frac{\mathrm{Iod_{LO}\,(BE)}}{\mathrm{I_{TO}\,(FE)}} \frac{\tau_{\mathrm{Iod}}}{\tau_{\mathrm{FE}}} \approx 10^4 \times \left(10^3/3\right) \cong 3 \times 10^6(!).$$

This is an extremely high enhancement factor. The concentration of residual iodine in a nominally pure sample AgBr is $\sim 10^{16}\,\mathrm{cm}^{-3}$. Considering the host lattice contains $\sim 6 \times 10^{22}$ molecules of AgBr per cubic centimetre, there is a single iodine ion per approximately 10^7 ions of the host lattice and, at the same time, 'its' own luminescence is by many orders of magnitude more intense than the intrinsic free exciton luminescence characterizing the pure host lattice! How is this possible?

In addition to the efficient trapping of free excitons itself (which has already been discussed when introducing the bound excitons at the beginning of Section 7.2), two other factors contribute to the high efficiency of the radiative recombination of an already trapped exciton. The first one is the absence of Auger non-radiative recombination. An exciton bound to a neutral donor or acceptor represents three quasi-particles localized in a relatively small volume—either two electrons and one hole or two holes and one electron. This promotes a high probability of Auger recombination, therefore the luminescence of BE at neutral donors and acceptors is not particularly intense. On the contrary, the third quasi-particle is missing in the case of an exciton in an isoelectronic trap, therefore, Auger recombination does not take place at all.

A second factor, important mainly in indirect-bandgap semiconductors (both AgBr and GaP), is the already mentioned strong localization of one quasi-particle at the impurity atom. The Heisenberg uncertainty relations $\Delta x \Delta k \geq 1/2$ (where Δx is the uncertainty in the spatial coordinate and Δk that in the wavevector) imply, however, that a strong localization in real space ($\Delta x \to 0$)

excitons have different symmetry and, secondly, in radiative recombination of the impurity centre also local vibrations may participate. More detailed discussion of the phonon structure of the AgBr/I luminescence can be found in Czaja, W. and Baldereschi, A. (1979). *J. Phys. C: Solid State Phys*., **12**, 405.

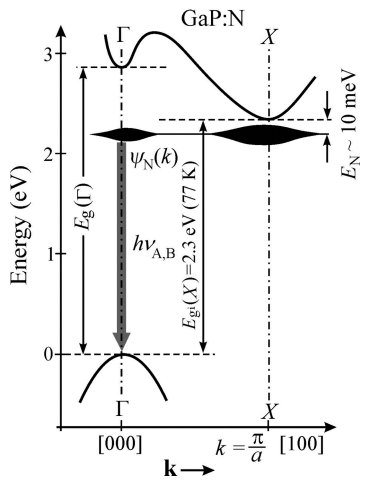

Fig. 7.27
Energy band structure of the GaP doped with nitrogen. Black filled areas denote the amplitude of the electron wavefunction $\psi_N(\mathbf{k})$. It is seen that $|\psi_N(\mathbf{k}=0)|^2 \neq 0$. Quasi-direct transitions at the Γ point lead to intense luminescence (the lines A and B in Fig. 7.26(a)). E_N stands for the binding energy of the electron at the isoelectronic trap N. After Holonyak *et al.* [45].

inevitably introduces a strong delocalization of the wavefunction in **k**-space. Figure 7.27 depicts the situation as can be visualized in the energy band scheme of GaP:N [45]. The uncertainty Δk in localization of the modulus squared of the wavefunction $|\psi_N(\mathbf{k})|^2$ of an electron trapped at the N atom, i.e. an electron occupying the energy level just below the conduction band minimum at $\mathbf{k} \cong \pi/a(100)$, extends up to the $\Gamma(\mathbf{k}=0)$ point. This makes *quasi-direct radiative recombination* of the electron with hole possible. The probability of such transitions—taking place without the need of phonon assistance—is naturally by several orders of magnitude higher than that of the indirect transitions. This leads therefore to an exceptionally intense luminescence even in indirect-bandgap materials.

It might be perhaps useful to emphasize once more the principal difference between the luminescence of shallow impurities (donors and acceptors) and the radiative decay of an exciton bound to an isoelectronic trap. At the shallow impurities, the electron or hole is attracted to a donor or acceptor, respectively, by the long-range Coulomb force. The emission spectrum of the exciton bound at a shallow impurity always bears the character of narrow lines. On the other hand, the isoelectronic trap captures the electron or hole through a short-range force and the wavefunction of the corresponding quasi-particle is strongly delocalized in momentum space. According to the type of the exciton–phonon interaction, the emission spectrum may take the form of either narrow lines (GaP, $S \cong 0$) or a phonon wing with a few phonon replicas in the case of medium exciton–phonon coupling (ZnTe/O, $S \cong 3$), or possibly a broad band in the case of very strong coupling (AgBr, $S \cong 9$).

The luminescence of the isoelectronic impurity N has found widespread use in the production of green-emitting electroluminescence diodes based on GaP/N. The emission spectrum of this kind of diode is shown in Fig. 7.28 [46]. In commercially produced diodes, ternary alloys $GaAs_{1-x}P_x$ ($x = 0.4$ to 1) are often used as the active medium which enables, apart from other things, the emission wavelength to be tuned. At high nitrogen doping, another radiative recombination channel due to the presence of coupled nitrogen atoms (NN-pair states) appears. A detailed discussion of the physics of the isoelectronic impurity N in $GaAs_{1-x}P_x$ can be found in the review article by Craford and Holonyak [47].

The question arises here as to whether it is possible to apply the principle of the isoelectronic trap also in homopolar semiconductors of group IV. It is a topical problem, in particular relevant to the search for light-emitting materials on a Si basis for future silicon photonics (Chapter 15). The doping of silicon with germanium or tin can hardly lead to any effect because the electronegativities of these chemical elements are almost the same ($X_{Si} = 1.9$; $X_{Ge} = 2.0$; $X_{Sn} = 2.0$). As for doping with carbon ($X_C = 2.6$), the desirable effect of strong luminescence is expected—according to what was explained above—to occur. Unfortunately, this is not the case. The carbon-related luminescence in crystalline silicon, represented by a narrow line at ~ 0.97 eV, is very weak and, moreover, in order to appear, the material must first be activated by electron beam irradiation. The reasons for this are not fully clear. Both the small atomic radius of the carbon atom and the weak exciton–phonon interaction have a possible role to play. A closer analysis of issues of isoelectronic traps in silicon can be found in [48].

7.2.4 Self-trapped excitons

In polar semiconductors with sufficiently strong exciton–phonon interaction, free exciton trapping can occur also in a pure and unperturbed crystal lattice. This process is called self-trapping or auto-localization of the exciton; radiative recombination of such a self-trapped exciton (STE) then evidently represents an *intrinsic luminescence process*. One can infer—from the fact that the exciton–phonon interaction is strong—that the corresponding luminescence emission spectrum will be broad.

An intuitive illustrative idea of exciton self-trapping can be drawn in the following way: the translational movement of the exciton through the lattice is driven by its heavier constituent, i.e. the hole. If the polaron coupling constant of the hole α_h is high, the hole–polaron is heavy; its effective mass is described by relation (6.9). The movement of the heavy hole is then very slow, the hole thus strongly polarizes the surrounding lattice, and thereby its movement is further slowed down and, finally, a total localization of the hole close to some atom constituting the host lattice can occur owing to positive feedback. A light electron accompanying the hole will then describe its orbit in the close vicinity.

A more exact phenomenological description of the self-trapping of free quasi-particles as well as that of the entire exciton was put forward by Toyozawa [49]. In the case of an electrically neutral particle—an exciton—the interaction with the host lattice is, according to Toyozawa, caused not directly by the electric forces but mainly by the short-range (s) forces, and a redistribution of atoms (lattice relaxation—LR) occurs in the close vicinity of the exciton. This redistribution is within the configurational coordinate model accompanied by the lattice relaxation energy E_R given by relation (4.14). For the purpose of more exact identification, we denote here this relaxation energy as E^s_{LR}; thus $E^s_{LR} = S_0\,\hbar\omega$, where S_0 is the Huang–Rhys factor. The short-range interaction is characterized by the parameter $g_s = E^s_{LR}/B$, where B is the total energy width of the exciton band.

The interaction of charged quasi-particles, electrons and holes, with the lattice is mediated by the Fröhlich mechanism employing LO-phonons. Consequently, long-range (ℓ) forces are involved and Toyozawa introduces the parameters E^ℓ_{LR} and $g_\ell = E^\ell_{LR}/B$ for their characterization. The Fröhlich interaction is naturally completely absent in homopolar semiconductors of group IV (Si, Ge), and therefore $g_\ell = 0$ there.

Toyozawa showed that excitons can occur really in two stable states that occupy local energy minima in the configurational coordinate model: free (F) and self-trapped (S) states. A self-trapped exciton gets localized in a potential well, created as a consequence of the strong lattice deformation over the exciton's surroundings. Toyozawa assigns this exciton to an effective mass $m' = m_{exc}\exp S_0$, where m_{exc} is the free exciton effective mass (thus the case of a strong exciton–phonon interaction, when $S_0 \gg 1$, entails $m' \to \infty$). The steady state switches rapidly from F to S as soon as the value of the coupling constant $g_s = E^s_{LR}/B$ exceeds unity.

The resulting phase diagram in the plane (g_s, g_ℓ) is shown in Fig. 7.29. The coupling of electrons, holes and excitons with phonons increases in the direction of rising g_s, g_ℓ. The F–S boundary is depicted by a solid line, and sections marked F(S) and S(F) indicate regions in which the self-trapped and free states

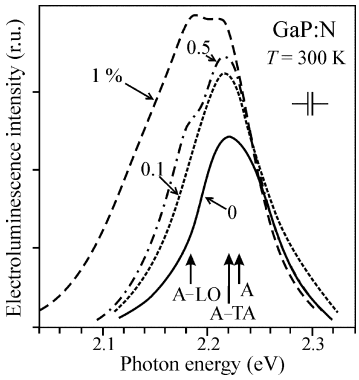

Fig. 7.28
Emission spectrum of the green electroluminescence from a GaP/N diode at room temperature. The GaN content in the melt is shown in percent at the individual curves. The positions of the individual lines from Fig. 7.26(a) are indicated; these lines merge into a single band at higher temperature. The red-shift of the lines in comparison with Fig. 7.26(a) is caused by the bandgap narrowing upon temperature increase 4 K → 300 K. After Vishnevskaya *et al.* [46].

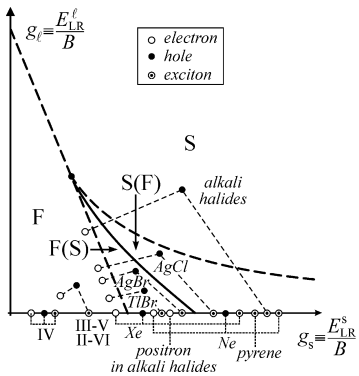

Fig. 7.29
Phase diagram in the (g_s, g_ℓ) plane for electrons, holes and excitons in a deformable lattice. The boundary F (free state)–S (self-trapped state) is depicted by a solid line. It is seen that self-trapping does not occur in IV, III-V and II-VI semiconductors. In AgCl and alkali halides, the hole and subsequently also the exciton become self-trapped. After Toyozawa [49].

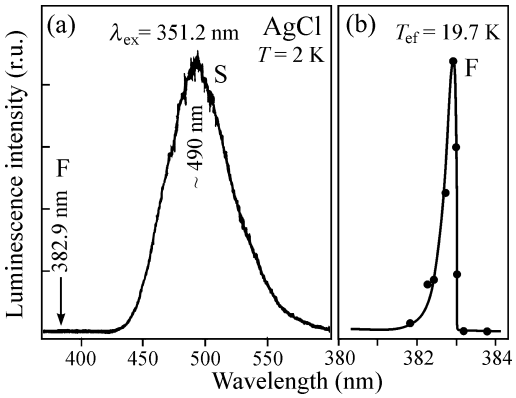

Fig. 7.30
(a) Emission spectrum of AgCl under pumping with laser pulses 351 nm (∼ 1 ps) at T = 2 K. The position of the expected free exciton luminescence line is indicated by the arrow F. The broad band S at ∼490 belongs to the self-trapped exciton. (b) Time integrated luminescence in the region of the expected free exciton emission. Its intensity is extremely weak (∼ 70 counts/s) and the luminescence decays very quickly (∼ 20 ps). This line has been attributed to the radiative decay of the free exciton. Points represent experiment; the full line is the Maxwell–Boltzmann shape (7.16) with an effective temperature of 19.7 K. After Kobayashi *et al.* [50].

can coexist (more details later). It can be clearly seen that a break occurs in silver halides—while both the carriers and the exciton are still free in AgBr (and also in TlBr), in AgCl the hole becomes self-trapped and, consequently, self-trapping of the exciton also occurs. Therefore, the luminescence of a (free) exciton in AgBr consists of a narrow resonant emission line (Fig. 7.15), while the emission spectrum of STE with $S_0 \geq 50 \gg 1$ in AgCl is represented by a broad band at ∼490 nm (Fig. 7.30(a) [50] or Fig. 4.10(c)). Although AgBr and AgCl differ very little only in most physical, chemical and photochemical properties, the difference in their low-temperature luminescence is substantial!

Various microscopic mechanisms of hole self-trapping can exist. In AgCl the hole becomes self-trapped—even though it may seem strange at first sight—at an already positively charged cation Ag^+[51], thereby a 'molecular ion' $(Ag^+Cl_6^-)^{4-}$ is created, see Fig. 7.31. The reason for such hole localization lies, in the first place, in the fact that the valence band maximum of AgCl at L_3' comprises contributions both from 3p states of Cl^- and 4d states of Ag^+; therefore the self-trapped hole must be constructed from both the states of chlorine and silver. The Jahn–Teller effect leads to a lowered symmetry of the created complex, because of lifting the geometrical equivalence of the six chlorine ions—four of them move towards the central Ag^{2+} ion while the other two move in the opposite direction. In this way a prolonged axis of the complex in one of the equivalent [100] directions is created (Fig. 7.31).[11]

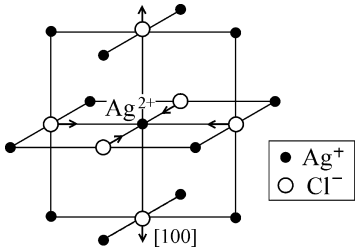

Fig. 7.31
Schematic of the microscopic structure of a self-trapped hole in AgCl depicting tetragonal distortion of the surrounding lattice. After von der Osten [51].

Free and self-trapped excitons may coexist. This holds true in segments marked as F(S) and S(F) in Fig. 7.29. One can imagine such coexistence in the framework of the configurational coordinate model as depicted in Fig. 7.32. In the particular case of AgCl, it is possible to interpret the configurational coordinate Q as the separation of Cl^- ligands from the central Ag^{2+} ion in the $(AgCl_6)^{4-}$ complex. The free exciton (minimum F in Fig. 7.32) is separated from the deeper minimum (S) of the self-trapped exciton by a potential barrier Δ. Free excitons created by light must overcome this barrier in order to reach the energetically favourable self-trapped state (by tunnelling at low temperatures); to do this, they need some time. Because the barrier is

[11] In alkali halides, on the other hand, the hole becomes self-trapped in the form of a molecular ion X_2^- (X = F, Cl, Br, I), which is the so-called V_k- centre oriented along the [110] direction.

low ($\Delta \cong 5$ meV) and thin in AgCl, it is easy to overcome. Therefore, the free exciton 'stays' in the F minimum only for a very short time and the probability of its radiative recombination there is negligible in comparison with penetrating the barrier and subsequently radiating an intense luminescence from the S minimum. In the standard steady-state luminescence experiment we thus record only a broad STE emission band at ~ 490 nm (Fig. 7.30(a)).

A time-resolved luminescence experiment taking advantage of short enough excitation pulses ($\sim$ 1 ps) together with a very sensitive detection system, however, permits us to verify the presence of an extremely weak emission line due to the free exciton radiative annihilation at the F minimum. Besides the fast pumping, also a sufficiently low temperature ($T = 2$–4 K) is necessary because higher temperatures rapidly promote the probability of thermally overcoming the barrier Δ. This delicate experiment was performed by Kobayashi and coworkers [50] and the result agreed exactly with expectation—they succeeded in detecting a weak line with spectral profile corresponding to the Maxwell–Boltzmann distribution at a wavelength of about 383 nm (which corresponds to the indirect exciton gap 3.248 eV decreased by the energy $\hbar\omega_{\mathrm{TO}} = 8$ meV of the quasi-momentum conserving phonon), see Fig. 7.30(b).

It is interesting to note that nanosecond pumping pulses are not sufficiently short for that purpose because the time required to penetrate the barrier appears to be very short, around 70 ps. However, also under pumping with relatively long ($\sim$10 ns) pulses time-resolved luminescence spectroscopy found a clear indication of short-living emission on the high-energy side of the STE emission band at $\sim$425 nm (Fig. 1.2(a)). This emission can be attributed to hot luminescence of STE (see the arrows H in Fig. 7.32) and to transient fusion of the free exciton with the self-trapped [52].

In general, the occurrence of exciton self-trapping in semiconductors is the exception rather than the rule. Experimental attention was, in addition to AgCl, paid to CdI_2 [53] and $ZnSe_{1-x}Te_x$ ($x \approx 0.01$) [54]. The latter case is, however, a ternary alloy containing defects of the disordered lattice that contribute significantly to the localization effect. Such a localization is no longer an intrinsic process, and is therefore called *extrinsic self-trapping* (the self-trapping occurs neither in pure ZnSe nor in pure ZnTe, in agreement with Fig. 7.29). Otherwise, it is possible to meet the intrinsic self-trapping of excitons in a variety of wide-bandgap non-semiconducting materials, both inorganic and organic. An overview of these phenomena is given in the monograph [55].

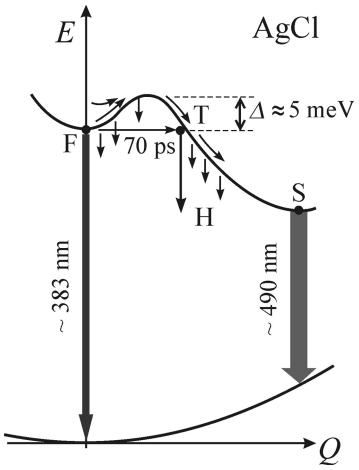

Fig. 7.32
Potential energy curve of a free (F) and self-trapped (S) exciton in the configurational coordinate model. Vertical lines depict luminescence processes, and Δ stands for the potential barrier against self-trapping. After Kobayashi *et al.* [50].

7.3 Problems

7/1: Show, employing the slope of the photon dispersion curve $\hbar c(\sqrt{\varepsilon_\infty})^{-1}$, that states corresponding to the polariton effects occupy within the first Brillouin zone only a very small volume around $\mathbf{k} = 0$. (This justifies why we consider $\hbar\omega(\mathbf{k} \cong 0)$ as the energy of phonons taking part in the thermalization and radiative recombination of the exciton–polariton, and it means also that the polariton effects play mostly a negligible role in the total emitted luminescence.)

7/2: Show that the maximum of the (X–LO) emission line is shifted from the energy of the free exciton ground state $n = 1$ towards lower energies not exactly by $\hbar\omega_0$, but by a temperature variable quantity $(\hbar\omega_0 – (3/2)k_B T)$.

7/3: The quasi-momentum conservation law is formulated differently depending on whether the free exciton radiative decay is one- or two-phonon assisted. This leads not only to a slightly different shape of the corresponding emission lines (eqns (7.12) and (7.13)) but also to different temperature dependences of both the lines. Show that the ratio of the integral intensities $I_{sp}^{(1)}$ and $I_{sp}^{(2)}$ of the X–LO and X–2LO lines, respectively, can be expressed as $(I_{sp}^{(1)})/(I_{sp}^{(2)}) = \gamma T$, where γ is a constant. Proceed from relations (7.12) and (7.13).

7/4: *Free excitons and the configurational coordinate model.* A free exciton, considering its translational movement, surely does not represent a localized luminescence centre. Can we discuss its luminescence behaviour in the framework of the configurational coordinate model? According to what was formulated in Section 4.4 obviously not. However, the existence of the LO-phonon assisted radiative decay of free excitons points to the fact that an intrinsic exciton–phonon interaction occurs here. We can then consider the (X–LO), (X–2LO), etc. lines as being phonon satellites of the resonant exciton–polariton (no-phonon) line. Therefore, also here we are in principle allowed to use formally the configurational coordinate model, and the reason for this is the finite spatial extent of the exciton wavefunction. The rise and decay of the related electronic polarization then causes a moderate lattice deformation. The Huang–Rhys factor S is, naturally, very small ($S \doteq 0.1$). Deal with the Huang–Rhys factor of free excitons after Zhao and Kalt [56].

7/5: We have derived the symmetry-driven selection rules for indirect exciton transitions in AgBr by making use of (7.17). The applied approach was, however, somewhat simplified. That is, we tacitly assumed the vertical photon-related transitions to the nearby 'virtual' states (whose involvement results from second-order perturbation theory) to be dipole allowed, see transitions $L_1 - L_3'$ and Γ_1–Γ_{15} in Fig. 7.33. Show, using relation (7.14), that this assumption was justified. (You need not know either the tables of characters of point groups or to be proficient in their usage. You will find all the necessary relations throughout Subsections 7.1.3 and 7.1.4. We recall only that $\Gamma_1 \otimes \Gamma_X = \Gamma_X$ holds for an arbitrary representation Γ_X, because the Γ_1 representation is spherically symmetric.)

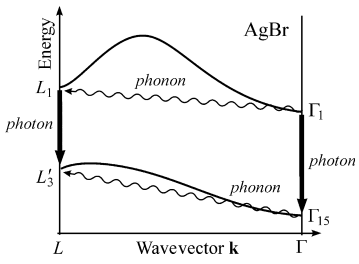

Fig. 7.33

References

1. Knox, R. S. (1963). *Theory of Excitons*. Academic Press, New York; Bassani, F. and Pastori Parravicini, G. (1975). *Electronic States and Optical Transitions in Solids*. Pergamon Press, Oxford.
2. Velický, B., Tauc, J., Trlifaj, M., and Prosser, V. (1965). *Interaction of electromagnetic radiation with solids* (In Czech: *Interakce elektromagnetického záení s pevnou látkou*). In *Solid State Theory* (In Czech: *Teorie pevných látek*), p. 229. NČSAV, Prague.

3. Klingshirn, C. F. (1995). *Semiconductor Optics*. Springer, Berlin.
4. Peyghambarian, N., Koch, S. W., and Mysyrowicz, A. (1993). *Introduction to Semiconductor Optics*. Prentice Hall, Englewood Cliffs, N.J.
5. Weisbuch, C. and Benisty, H. (2005). *phys. stat. sol. (b)*, **424**, 2345.
6. Joesten, B. L. and Brown, F. C. (1966). *Phys. Rev.*, **148**, 919.
7. Razeghi, M., Omnes, F., Nagle, J., Defour, M., Acher, O., and Bove, P. (1989). *Appl. Phys. Lett.*, **55**, 1677.
8. Koteles, E. S., Lee, J., Salerno, J. P., and Vassel, M. O. (1985). *Phys. Rev. Lett*., **55**, 867.
9. Bose, S. S., Kim, M. H., and Lee, B. (1988). *J. Electr. Mater.*, **17**, S36.
10. Gross, E., Permogorov, S., and Razbirin, B. (1966). *J. Phys. Chem. Solids*, **27**, 1647.
11. Segall, B. and Mahan, G. D. (1968). *Phys. Rev.*, **171**, 935.
12. Gross, E. F., Permogorov, S. A., and Razbirin, B. S. (1971). *Sov. Phys. Usp.*, **14**, 104.
13. Bassani, F. and Pastori-Parravicini, G. (1975). *Electronic States and Optical Transitions in Solids*. Pergamon Press, Oxford.
14. Kunz, A. B. (1982). *Phys. Rev. B*, **26**, 2070.
15. von der Osten, W. and Weber, J. (1974). *Solid State Comm.*, **14**, 1133.
16. Thomas, G. A., Frova, A., Hensel, J. C., Miller, R. E., and Lee, P. A. (1976). *Phys. Rev. B*, **13**, 1692.
17. Hensel, J. C., Phillips, T. G., and Thomas, G. A. (1977). *The electron–hole liquid in semiconductors: experimental aspects*. In *The Electron–Hole Liquid in Semiconductors* (ed. H. Ehrenreich, F. Seitz and D. Turnbull), p. 88. *Solid State Physics* Vol. 32. Academic Press, New York.
18. Rashba, E. I. and Gurgenishvili, G. E. (1962). *Sov. Phys. – Solid State*, **4**, 759.
19. Haynes, J. R. (1960). *Phys Rev. Lett.*, **4**, 361.
20. Bebb, H. B. and Williams, E. W. (1972). *Photoluminescence I. Theory*. In *Semiconductors and Semimetals* (ed. R. K. Willardson and A. C. Beer), Vol. 8, p. 181. Academic Press, New York and London,
21. Bernussi, A. A., Barreto, C. L., Carvalho, M. M. G., and Motisuke, P. (1988). *J. Appl. Phys.*, **64**, 1358.
22. Hayes, W. and Stoneham, A. M. (1985). *Defects and Defect Processes in Nonmetallic Solids*. John Wiley, New York.
23. Hönerlage, B., Rössler, U., and Schröder, U. (1975). *Phys. Rev. B*, **12**, 2355.
24. Herbert, D. C. (1984). *J. Phys. C: Solid State Phys.*, **17**, L901.
25. Kaminskii, A. S. and Pokrovskii, Ya. E. (1970). *JETP Lett.*, **11**, 255.
26. Lampert, M. A. (1958). *Phys. Rev. Lett.*, **1**, 450.
27. Kirczenow, G. (1977). *Canad. J. Phys.*, **55**, 1787.
28. Tajima, M.(1982). *Quantitative impurity analysis in Si by the photoluminescence technique*. In *Semiconductor Technologies* (ed. J. Nishizawa), p. 1. North Holland, Amsterdam.
29. Pelant, I., Hála, J., Ambrož, M., Vácha, M., Valenta, J., Adamec, F., Kohlová, V., and Matoušková, J. (1990). *Impurity analysis in Si crystals by the photoluminescence method V* (In Czech*: Analýza přiměsí v krystalech Si fotoluminiscenční metodou V*). Research Report for Tesla Rožnov, k.p., Charles University in Prague, Faculty of Mathematics & Physics, Prague.
30. Colley, P. McL. and Lightowlers, E. C.(1987). *Semicond. Sci. Technol.*, **2**, 157.
31. Pelant, I., Hála, J., Ambrož, M., Kohlová, V., and Vacek, K. (1989). *Czech. J. Phys A* (In Czech), **39**, 142.
32. Karaiskaj, D., Thewalt, M. L. W., Ruf, T., and Cardona, M. (2003). *phys. stat. sol. (b)*, **235**, 63.
33. Pelant, I., Hála, J., Ambrož, M., and Kohlová, V. (1988). *Photoluminescence of impurities and photoluminescence assessment of boron and phoshorus in silicon* (In Czech: *Fotoluminiscence přiměsí a fotoluminiscenční stanovení boru a fosforu v křemíku*). In *Křemík '88*, part 2, p. 86. General Head Office Tesla–ES, Rožnov pod Radhoštěm.

34. Pelant, I., Hála, J., Ambrož, M., and Kohlová, V. (1988). *Quantitative analysis of low concentrations of boron and phosphorus in silicon by the laser luminescence spectroscopy—experimental aspects* (In Czech: *Kvantitativní analýza nízkých koncentrací boru a fosforu v křemíku laserovou luminiscenční spektroskopií – experimentální aspekty*). In *Lasers in Research and Industry* (6th Czechoslovak Conference), p. 252. Račkova dolina, SVŠT ČSSP Liptovský Mikuláš.
35. Kaminskii, A. S., Kolesnik, L. I., Leiferov, B. M., and Pokrovskii, Ya. E. (1982). *J. Appl. Spectros.*, **36**, 516.
36. Schumacher, K. L. and Whitney, R. L. (1989). *J. Electron. Mater.*, **18**, 681.
37. Broussell, I., Stolz, J. A. H., and Thewalt, M. L. W. (2002). *J. Appl. Phys*., **92**, 5913.
38. Zimmermann, H., Boyn, R., Michel, C., and Rudolph, P. (1990). *phys. stat. sol.* (*a*), **118**, 225.
39. Thewalt, M. L. W., Nissen, M. K., Beckett, D. J. S., and Lungren, K. R. (1989). *High-performance photoluminescence spectroscopy using Fourier-transform interferomety*, MRS Meeting Boston November/December, Symp. G. *MRS Symposium Proceedings*, **163**, (1990), 221.
40. Dekker, A. J. (1963). *Solid State Physics*. Prentice-Hall, Englewood Cliffs, N.J.; Curie, D. (1960). *Luminescence Cristalline*. Dunod, Paris.
41. Gershoni, D., Cohen, E., and Ron, A. (1985). *J. Luminescence*, **34**, 83.
42. Pelant, I. (1988). *Laser luminescence spectroscopy of some crystalline semiconductors and ionic crystals* (In Czech: *Laserová luminiscenční spektroskopie vybraných krystalických polovodičů a dielektrik*), DSc Thesis, Charles University in Prague, Faculty of Mathematics and Physics, Prague.
43. Tsukakoshi, M. and Kanzaki, H. (1971). *J. Phys. Soc. Japan*, **30**, 1423.
44. Stolz, H., von der Osten, W., and Weber, J. (1976). *Lifetime and time-resolved spectra of indirect excitons in AgBr*. In *Physics of Semiconductors* (ed. F. G. Fumi), p. 865. *Proceedings of the 13th International Conference on the Physics of Semiconductors*, Rome.
45. Holonyak, N. Jr., Campbell, J. C., Lee, M. H., Verdeyen, J. T., Johnson, W. L., Craford, M. G., and Finn, D. (1973). *J. Appl. Phys*., **44**, 5517.
46. Vishnevskaya, B. I., Korneev, V. M., Kogan, L. M., and Yunovich, A. E. (1973). *Soviet Phys. Semicond.*, **6**, 1372.
47. Craford, M. G. and Holonyak, N. Jr. (1976). *The optical properties of the nitrogen isoelectronic trap in* $GaAs_{1-x}P_x$. In *Optical Properties of Solids. New Developments* (ed. B. O. Seraphin), p. 187. North Holland, Amsterdam.
48. Brown, T. G. and Hall, D. G. (1998). *Radiative isoelectronic impurities in silicon and silicon–germanium alloys*. In *Light Emission in Silicon: From Physics to Devices* (ed. D. J. Lockwood), *Semiconductors and Semimetals* Vol. 49, p. 77. Academic Press, San Diego.
49. Toyozawa, Y. (1970). *J. Luminescence*, **1**, 632; Toyozawa, Y. (1981). *J. Luminescence*, **24/25**, 23.
50. Kobayashi, M., Matsushima, Y., Nishi, O., Mizuno, K., and Matsui, A. H. (1995). *SPIE*, **2362** (*Exciton processes in condensed matter*), 225.
51. von der Osten, W. (1984). *Excitons and exciton relaxation in silver halides*. In *Polarons and Excitons in Polar Semiconductors and Ionic Crystals* (ed. J. T Devreese and F. Peeters), p. 293. Plenum Press, New York.
52. Pelant, I. and Hála, J. (1991). *Solid State Comm.*, **78**, 141.
53. Nakagawa, H., Muneda, Y., and Matsumoto, H. (1988). *J. Luminescence*, **40/41**, 485.
54. Lee, D., Mysyrowicz, A., Nurmikko, A. V., and Fitzpatrick, B. J. (1987). *Phys. Rev. Lett.*, **58**, 1475.
55. Song, K. S. and Williams, R. T. (1996). *Self-Trapped Excitons*. Springer Series in Solid State Sciences Vol. 105. Springer, Berlin.
56. Zhao, H. and Kalt, H. (2003). *Phys. Rev. B*, **68**, 12.